Chemical routes to materials

Carbon materials with high pentagon density

Nooramalina Diana[1], Yasuhiro Yamada[2,*] , Syun Gohda[2,3], Hironobu Ono[3], Shingo Kubo[4], and Satoshi Sato[2]

[1] *Faculty of Engineering, Chiba University, 1-33 Yayoi, Inage, Chiba 263-8522, Japan*

[2] *Graduate School of Engineering, Chiba University, 1-33 Yayoi, Inage, Chiba 263-8522, Japan*

[3] *Nippon Shokubai Co., Ltd, 5-8 Nishiotabi, Suita, Osaka 564-0034, Japan*

[4] *Research Support Center, Kagoshima University, 1-21-40 Korimoto, Kagoshima 890-0065, Japan*

ABSTRACT

Pentagons in carbon materials have attracted attentions because of the potential high chemical reactivity, band gap control, and electrochemical activity. However, it is challenging to prepare a carbon film with high pentagon density because of the curvature and the high reactivity caused by the presence of pentagons, and it is also challenging to estimate the percentage of pentagons in carbon materials because of the limitation of current analytical techniques. In this work, the percentage of pentagons in carbon materials was experimentally estimated for the first time using experimental and calculated C1s X-ray photoelectron spectroscopy and elemental analysis. Carbon films with 7% of pentagons (40% of pentagons compared to the raw material) with electrical resistivity of 1.1×10^4 Ω meter were prepared by heat treatment of corannulene at 873 K. On the other hand, fluoranthene and fullerene remained as non-film solid and powder without forming films at 873 K. Experimental and calculated Raman and IR spectra revealed the peaks of different types of pentagons. Decrement of pentagons in corannulene and fluoranthene heated at high temperatures can be explained mainly by the scission of C=C bond in pentagons, as suggested by the results of reactive molecular dynamics simulation (ReaxFF).

GRAPHIC ABSTRACT

Introduction

Since the discovery of fullerene in 1985 [1] and the observation of carbon nanotube in 1991 [2], pentagons have attracted the greatest attention in the field of carbon materials. Since the groundbreaking research of graphene in 2004 [3, 4], researchers have developed a new generation of carbon materials to improve the performance of various applications by introducing defects such as pentagons, heptagons [5–7], zigzag and armchair edges [8–11], and functional groups [12, 13]. For example, it has been reported that carbon materials with pentagons and zigzag edges have high reactivity [5, 11, 14, 15], high activities for oxygen reduction reaction of fuel cell [15], and can be utilized to adjust band gaps of graphene nanoribbon [16]. It is also possible that the introduction of those defects has effect on the other applications and phenomena such as bioimaging and electromagnetic interactions [17, 18]. The various properties can be further enhanced significantly by increasing the density of defects such as pentagons.

Graphene nanoribbons with controlled edges such as zigzag and armchair edges have been synthesized on metal substrates, which work as catalysts [8, 9]. Coexistence of heptagons or octagons with pentagons such as Stone–Thrower–Wales defects (5-7-7-5 rings) and grain boundaries [19, 20] flattens graphene in the

presence of pentagon. Thus, it is possible to synthesize graphene with the mixed defects in the form of a flat sheet. However, the synthesis of carbon materials with high pentagon density in the form of a film on a metal substrate is still challenging because the introduction of pentagons generates curvature in the absence of other defects and the carbon films with pentagons do not contact the metal substrate parallelly.

Carbon materials with high pentagon density have been studied for decades because of the increment of the interest in the bottom-up synthesis of fullerene [21, 22] and related fullerene-like carbon materials [5, 23–25]. For example, polymerization of fullerene has been reported, but either electron beam [23] or high pressure [24, 25] was necessary for the polymerization. Also, carbon materials with high pentagon density prepared by alkaline etching of fullerene have been reported, but uncontrolled oxygen-containing functional groups were introduced during the etching [5]. Our recent studies aimed at preparing carbon materials with zigzag and armchair edges have also shown the presence of pentagons by carbonizing polyaromatic compounds such as tetracene. However, the percentage of pentagons in the carbon materials has not been discussed [11] because of the difficulty to estimate the percentage.

Corannulene with one pentagon surrounded by 5 hexagons (Figs. 1a and 2ai) has recently become

Figure 1 Structure of corannulene and possible structures of carbonized corannulene. **a** Corannulene. **b** Dehydrogenated corannulene. **c** Carbonized corannulene.
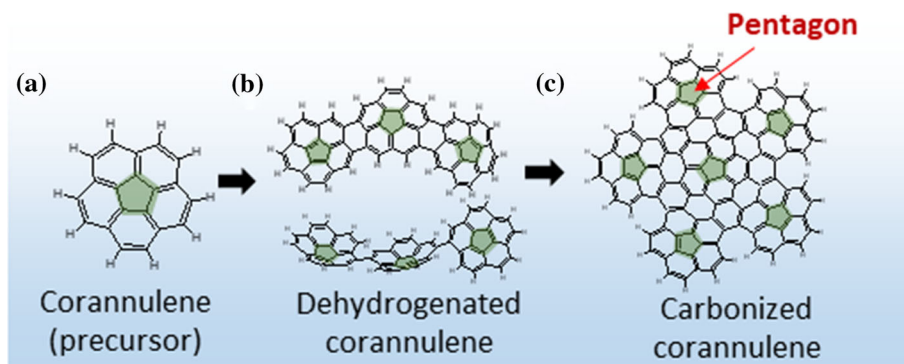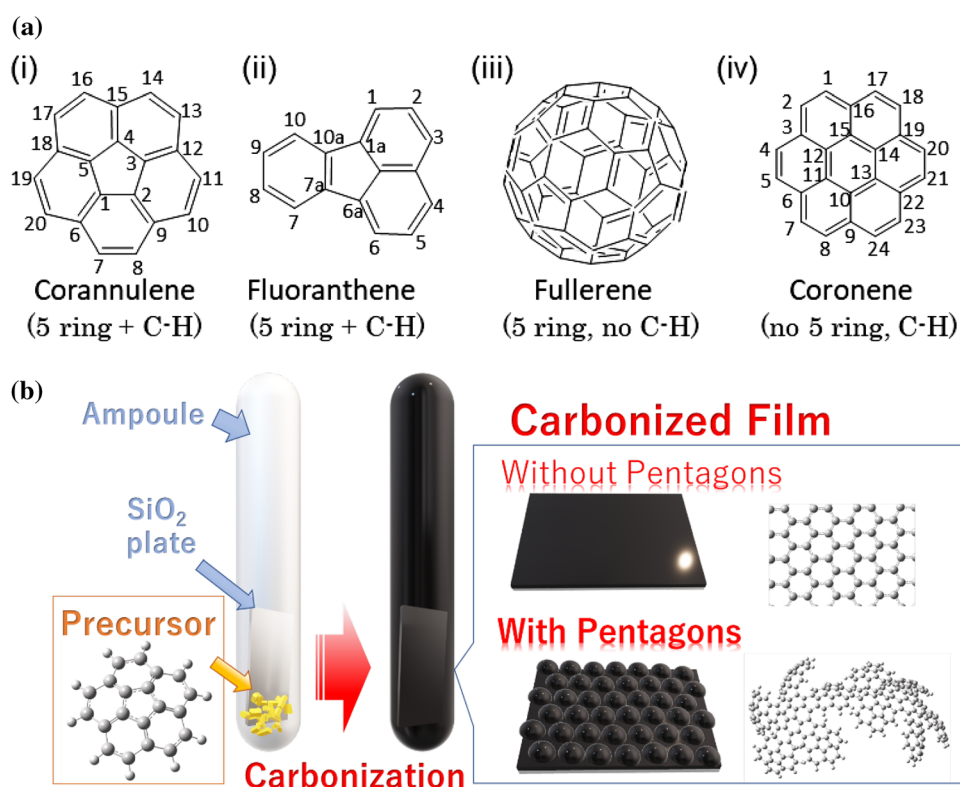

Figure 2 Structures of raw materials (**a**) and a preparation method of this work in an ampoule (**b**). **ai** Corannulene. **aii** Fluoranthene. **aiii** Fullerene. **aiv** Coronene. **b** Preparation method. Quartz plates were placed in ampoules to prepare carbonized films. White sphere: hydrogen atom. Gray sphere: carbon atom.

attractive as a raw material of nanocarbon materials because of the unique structure and properties such as electron accepting capability and charge carrying capability [26, 27] and possibility to store a large amount of lithium between corannulene molecules for lithium ion battery [28]. Corannulene trimer and other related nanocarbon materials with pentagons have been prepared by organic chemical synthesis [26, 29, 30] and laser [31]. However, preparation of carbon films with high pentagon density from corannulene by heat treatment has not been reported to the best of our knowledge.

Even if carbon materials with pentagons were prepared, it is still challenging to analyze the structures of carbon materials with pentagons quantitatively. For example, carbonization of aromatic compounds with pentagons such as acenaphthylene has been reported by several groups [32–34] and summarized by Granda et al. [35] and Mochida et al. [36]. In particular, Mochida et al. reported carbonization of various compounds with pentagons such as acenaphthylene, acenaphthene, decacyclene, truxene, fluorene, and fluoranthene with/without aluminum chloride at 723 and 873 K on substrates, and observed under optical microscope, but the detailed reaction steps were not explained except for acenaphthylene [36]. In the proposed reaction steps, pentagons were completely removed at 753 K and

turned into hexagons. In addition, carbon films were partially coated on substrates. Unlike acenaphthylene, whose pentagon is surrounded by only two hexagons, pentagons in corannulene and fluoranthene used in this work are surrounded by more than three hexagons. Because of the absence of reactive pentagonal C-H in corannulene and fluoranthene, the reaction steps of corannulene and fluoranthene compared to that of acenaphthylene are completely different. In the paper, three kinds of reaction routes were proposed for carbonization of acenaphthylene, in addition to the disappearance of the pentagon at 613–753 K.

Aberration-corrected transmission electron microscope (TEM) [20] can be used for observation of reaction steps inside carbon nanotube [37]. However, the aberration-corrected TEM can be utilized to observe only limited area and it is not suitable for carbon materials with more than three layers of graphene-like structures. Nuclear magnetic resonance and neutron diffraction are possible techniques to estimate the pentagon [38–40], but a large amount of gram-scale samples is necessary. Raman spectroscopy is generally utilized to confirm the presence of pentagons in carbon materials because it requires small amount of sample, but the percentage of pentagons cannot be estimated clearly. Our group has recently developed a quantitative analytical method to estimate the percentage of pentagons in graphene [41] in addition to qualitative analytical methods of oxygen- [14, 42, 43], nitrogen- [10, 44, 45], sp^3C-, and sp^2C- [46], zigzag edge-, and armchair edge-containing [47] and metal ion-coordinated [48] carbon materials by X-ray photoelectron spectroscopy (XPS) with the aid of density functional theory (DFT) calculation.

Understanding carbonization mechanisms is also essential to clarify the reason for the remained high pentagon density in carbonized films. Utilization of molecular dynamics (MD) simulation with reactive force field (ReaxFF) has been recently utilized to estimate the carbonization and related reaction mechanisms by several researchers [49, 50] including our group [10, 11, 51]. ReaxFF can estimate the carbonization mechanisms computationally, but the experimental approaches to reveal the mechanisms are also necessary. Infrared (IR) spectroscopy has been known to be one of the powerful tools to determine the edge structures of carbon materials (Fig. 3) [10, 11, 51, 52], in addition to the

conventionally utilized Raman spectroscopy [11, 53–56]. In particular, assignments of IR spectra for aromatic compounds and carbon materials with/without pentagons by comparing experimental and calculated spectra are shown in our previous work [40]. It is expected that carbonization steps of carbon materials with high pentagon density can also be verified using these techniques.
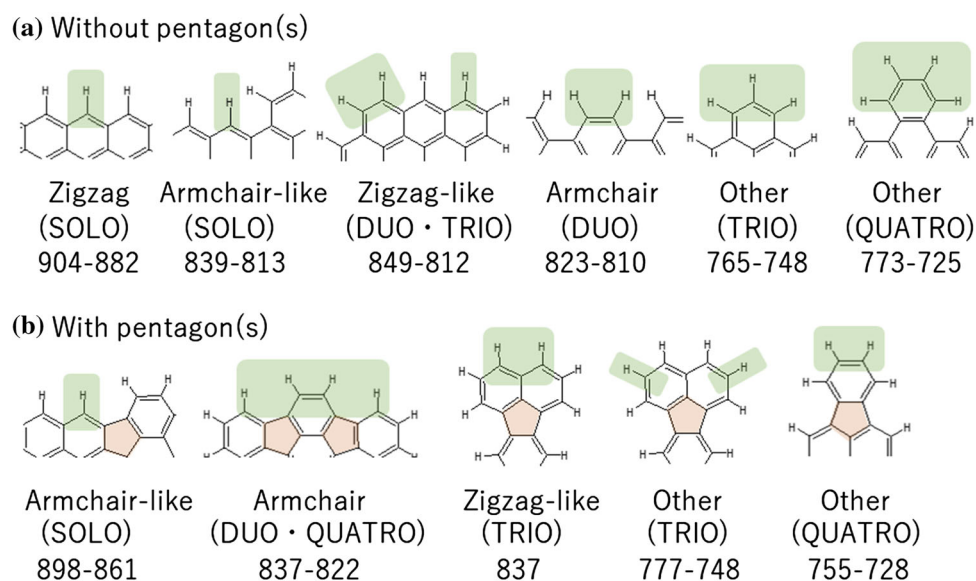
In this work, carbon films with high pentagon density were prepared by heat treatment in ampoules (Fig. 2b), and the reasons for the presence of high pentagon density in carbon films were revealed by comparing carbonization mechanisms of four raw materials such as corannulene with one pentagon and C-H groups (Fig. 2ai), fluoranthene with one pentagon and C–H groups (Fig. 2aii), and fullerene with one pentagon and no C–H group (Fig. 2aiii), and coronene without pentagons and with C–H groups (Fig. 2aiv). To verify the presence of pentagons in carbon materials and the plausible carbonized structures, experimental analyses and DFT calculation of IR spectroscopy, Raman spectroscopy, and ReaxFF were conducted. Experimental and calculated XPS analyses with the aid of experimental elemental analysis were also conducted to estimate the percentage of pentagons in carbonized films. In addition, the carbonization reactivities of four raw materials were compared and the reason for the difference in reactivity of four raw materials was discussed from the aspect of orbitals, formation energies of radicals, and bond length.

Experimental and simulation

Preparation

Corannulene (purity > 97.0%, melting point 542 K), fluoranthene (purity > 98.0%, melting point 381–385 K), and coronene (purity > 95.0%, melting point 713 K) were purchased from Tokyo Chemical Industry Co., Ltd., Japan, and fullerene (purity: not available) was purchased from Kanto Chemical Co., Inc., Japan (Fig. 2a). These compounds were used without further purification. One of raw materials (20 mg) was packed together with quartz plates [$6 \times 6 \times 1$ (mm)^3 and $20 \times 5 \times 1$ (mm)^3] in an ampoule and heated in vacuum for 1 h at temperatures between 773 and 1273 K depending on the carbonization temperatures of each raw material

Figure 3 Definitions of edge structures of carbon materials assigned using IR spectra by our group [52].

(a) Without pentagon(s)

| Zigzag (SOLO) 904–882 | Armchair-like (SOLO) 839–813 | Zigzag-like (DUO · TRIO) 849–812 | Armchair (DUO) 823–810 | Other (TRIO) 765–748 | Other (QUATRO) 773–725 |

(b) With pentagon(s)

| Armchair-like (SOLO) 898–861 | Armchair (DUO · QUATRO) 837–822 | Zigzag-like (TRIO) 837 | Other (TRIO) 777–748 | Other (QUATRO) 755–728 |

(Fig. 2b). Carbonization temperatures in this work mean that the carbon-rich materials were formed by heat treatment [57]. The quartz plates were used as substrates to obtain flat films for measuring XPS spectra and electrical resistivity. The heat-treated sample was further heated under reduced pressure at a temperature higher than the melting point of the corresponding raw material by 50 K to remove any remaining unreacted raw material in the sample.

Characterization

Samples were analyzed by Raman spectroscopy (NRS-4500 JASCO Corp., excitation laser wavelength; 532 nm for raw materials and 785 nm for carbonized samples), diffuse reflectance infrared Fourier transform (DRIFT) spectroscopy (FT-IR-4200, JASCO Corp., detector of MCT_M, resolution of 4 cm^{-1}, cumulated number of 32 times), elemental analysis (CE-440F, Exeter Analytical, Inc.), and XPS using MgKα (X-ray Gun: emission 10 mA, anode 10 kV. Photon energy: 1253.6 eV. Analyzer: hybrid lens, pass energy 40 eV. Neutralization condition: filament current of 1.75 A, and charge balance of 3.0 V, filament bias of 1.0 V. Axis Ultra Dld, Shimadzu Corp.). Neutralization was conducted in this work because of the use of raw materials and quartz plates as substrates with low electrical conductivity. For C1s XPS spectra, samples were coated on quartz plates by vaporizing the raw materials in quartz ampoules upon heat treatment except for as-received corannulene and coronene (Fig. 2b). Background subtraction

of C1s XPS spectra was performed using the Shirley method. Intensities of experimental C1s XPS spectra were normalized to 1 for comparison. The peak positions of C=C in experimental C1s spectra were adjusted to 284.3 eV [42–44] with the aid of results of calculated C1s XPS spectra and experimental elemental analyses conducted by combustion analysis.

The detailed analytical method combining elemental analysis and C1s XPS spectra is as follows. First, the calculated C1s XPS peak positions of C=C and C–H were applied to the experimental ones and the experimental peak positions were fixed. The atomic percentages of C and H obtained from experimental elemental analyses were applied to the peak area of C=C and C–H in experimental C1s XPS spectra. In this approach, one carbon atom in C=C was counted as one carbon atom and one carbon atom in C–H was counted as one carbon atom and one hydrogen. The results of experimental elemental analyses were used to analyze the percentages of C–H and C=C in experimental C1s XPS spectra because of the high accuracy of the atomic percentage of experimental elemental analyses for carbon and hydrogen. This is because the experimental C1s XPS spectra have close binding energy peak positions between C–H and C=C, and the percentages of C–H and C=C cannot be determined directly from the C and H atomic percentages [41–46]. C=C can be further divided into C=C in pentagons and that in hexagons. The percentages of C=C in pentagons and hexagons can be estimated by fixing the experimental

peak positions of C=C in pentagons and hexagons using the calculated ones.

Experimental IR, Raman, and XPS spectra of raw materials and carbonized samples were compared to the calculated spectra of raw materials and plausible carbonized structures as explained later. Surface morphology of carbon films and thickness of the cross section were observed under SEM (JEOL-6510, Jeol Ltd.) in order to understand the results of electrical resistivity. Electric current was analyzed to obtain electrical resistivity by Digital Multimeter (GWINSTEK GDM-8261A, Texio Technology Corp.) by applying voltage from 0–650 V using regulated DC power supply (TP0650-01D, Takasago, Ltd.). The two-probe method was used because the electrical resistivity was high enough and the contact resistivity was negligible. The method was also used because samples tend to contain cracks, as shown in the SEM images later, due to the shrinkage of samples upon carbonization on quartz plates and the two-probe method can avoid inclusion of cracks in the data of electrical resistivity measurement.

Calculation

Simulation of Raman, IR, and XPS spectra

In a similar way to our previously reported papers regarding Raman and IR [10, 11, 14, 45, 47, 48, 51, 52] and XPS [14, 41–46], Raman, IR, and XPS spectra of raw materials and plausible carbonized structures were simulated using Gaussian 09 [58]. The modeled structures were optimized and those IR and Raman spectra were simulated using either B3LYP/sto-3 g or B3LYP/b3lyp freq = Raman integral = grid = ultrafine. Scaling factors of B3LYP/6-31 g(d) to simulate IR and Raman spectra of small molecules were obtained from our previous work by comparing experimental and calculated spectra [11]. Scaling factors of B3LYP/sto3g to simulate IR and Raman spectra of large molecules were 0.892, which is a generally reported value [59]. Calculated peak positions were further shifted to adjust calculated positions to experimental ones. These scaling factors and shifts are summarized in Table S1 in Supplementary Materials. C1s XPS spectra were simulated using B3LYP/6-31 g(d) integral = grid = ultrafine pop = full gfprint. Orbital energies were obtained and the number of orbitals was plotted against orbital energies. The orbital energies were used as binding

energies of the calculated XPS spectra after applying the following scaling factors. As described in our previous studies [42, 43], scaling factors (The first scaling factor: 1.024 = 284.3/277.6. The third scaling factor: 1.35) were applied to adjust the peak positions of calculated XPS spectra to those of experimental XPS spectra. In addition, asymmetric Voigt-type function was applied to obtain spectra with full width at half maximum (FWHM) [41–46]. The minimum FWHM of the calculated C1s XPS spectra was obtained from the experimental XPS spectrum of graphite [42]. Applying experimental FWHM of the XPS spectrum of graphite to the calculated FWHMs of XPS spectra facilitates the discussions of spectral shape. Charge and spin multiplicity were set to 0 and 1, respectively. More detailed conditions for simulating IR and Raman spectra are shown in Table S1.

Calculation of formation energy, Mulliken charge, bond distance, natural bond orbital (NBO) analysis, molecular orbital, orbital energy, and band gap

Modeled structures were optimized, and formation energy, Mulliken charge, and bond distances were calculated using opt integral = grid = ultrafine B3LYP/6-31 g(d) in Gaussian 09 [58]. Formation energies of radicals were obtained from the difference between the energies before and after the formation of two radicals such as the radical of polycyclic aromatic hydrocarbon (PAH) and the radical of hydrogen using the following equation (Eq. 1).

$$E_{\mathrm{Formation}} = (E_{\mathrm{PHradical}} + E_{\mathrm{Hradical}}) - E_{\mathrm{PAH}} \qquad (1)$$

where $E_{\mathrm{Formation}}$ is the total electron energy of the formation for the PAH radical and the hydrogen radical, $E_{\mathrm{PAH\ radical}}$ is the total electron energy of PAH with one radical after removal of one hydrogen radical, $E_{\mathrm{H\ radical}}$ is the total electron energy of one hydrogen radical, and E_{PAH} is the total electron energy of the PAH. Charge and spin multiplicity for calculating one molecule with one radical were set as 0 and 2, respectively. NBO calculation was conducted under the same conditions using pop = nboread after optimizing the structures. All of molecular orbitals, orbital energies of the highest occupied molecular orbital (HOMO) and next HOMO (NHOMO), and band gaps between HOMO and the lowest unoccupied molecular orbital (LUMO) were calculated at the same conditions using B3LYP/6-31 g(d)

integral = grid = ultrafine pop = full gfprint after optimizing structures.

MD simulation with reactive force field

100 Molecules of corannulene, fluoranthene, and coronene and 35 molecules of fullerene were randomly positioned in a space with $3.5 \times 3.5 \times 3.5$ $(nm)^3$ using a builder function in ReaxFF (software name: ADF package released in 2016). Using ReaxFF (Force field containing London dispersion correction terms: "dispersion/CHONSSi-lg.ff" [60], Method: Velocity Verlet + Berendsen, Distance between molecules: 2.5 Angstrom), these compounds were heated from 0 to 3000 K at a heating rate of 10 K per each time step (0.1 fs).

Results and discussion

Appearance and elemental analysis of heat-treated compounds

Table 1 shows the changes in appearance and compositions of corannulene, fluoranthene, fullerene, and coronene after heat treatment. The appearance of corannulene changed from a yellow powder (composition: $C_{20}H_{10}$) to a black solid at 773 K ($C_{20}H_{8.1}$). At 823 K ($C_{20}H_{7.2}$) or higher, black films were formed on the wall of ampoules. Similarly, fluoranthene ($C_{16}H_{10}$) and coronene ($C_{20}H_{12}$) also changed their color into brown at 873 and 823 K and then black films were formed on the wall of ampoules at 903 K ($C_{16}H_{7.3}$) and 923 K ($C_{20}H_{7.2}$), respectively. The carbonized temperature [57] of corannulene was the lowest (823 K) among those of four raw materials because dehydrogenation proceeded at the lowest temperature. In addition, the change of appearance from yellow powder to black film was also observed. By comparing at similar degree of dehydrogenation for each sample, i.e., $C_{20}H_{7.2}$ (corannulene at 873 K), $C_{16}H_{7.3}$ (fluoranthene at 903 K), and $C_{20}H_{7.2}$ (coronene at 923 K), the temperature of corannulene was the lowest. The reason for the low dehydrogenation temperature of corannulene is explained later. The correlation between the loss of hydrogen and the change in color of heat-treated aromatic compounds, such as tetracene [11, 52], chrysene [11, 52], coronene [52], aromatic compounds with ethynyl and vinyl groups [10], and those with heteroatoms [10, 45] and
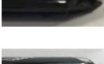
one pentagon [45], has been reported by our group as mainly because of the extension of conjugated systems by dehydrogenation. Carbonization of aromatic compounds containing only sp^2C such as tetracene, chrysene, and coronene basically proceeds by dehydrogenation reaction with or without going through the formation of sp^3C [11, 52]. It has been reported that the extension of the conjugated system, which correlates with low C–H in carbon materials, is associated with the low 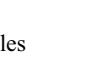band gaps and shift the peak position to higher wavelength of ultraviolet–visible absorption spectra [61]. The correlation of extension of conjugated systems and low C–H in carbon materials will be explained later from the point of view of band gap and electrical resistivity in this work.

Fluoranthene and coronene were carbonized at 903 and 923 K, respectively. On the other hand, the appearance of fullerene has remained as black powder even after the heat treatment at 1173 K because of the absence of C–H bonding in fullerene and the stable symmetric spherical structure of fullerene. It has been reported that the polymerization reaction of fullerene requires either electron beam [23] or high pressure [24, 25]. Also, coalescence of two carbon nanotubes into one carbon nanotube requires 1073 K in addition to the energy of electron beam [62]. In addition, coalescence of fullerene requires temperatures higher than 1073 K [63]. Thus, the presence of C–H is indispensable for carbonizing raw materials at 923 K or lower.

Bond length, molecular orbitals, total electron energy, and formation energy of radicals.

The reason for the high reactivity of corannulene among all the raw materials can be explained by the presence of C–H groups, C=C bond length (Fig. 4a), and molecular orbitals (Fig. 4b) combined with the concept of Clar's rule [64, 65], rather than Mulliken charge and hybridization calculated by NBO analysis (Figures S1 and S2). The C=C bond length between one carbon atom at the DUO position and one carbon atom at the valley position of coronene was 0.1424 nm (Fig. 4a4), which is close to the bond length of C=C in graphite (0.142 nm) [66]. The C=C bond length of one carbon atom at the TRIO position and one carbon atom at the valley position of fluoranthene was also 0.1424 nm (Fig. 4a2). On the other

Table 1 Appearance and composition of heat-treated corannulene, fluoranthene, coronene, and fullerene

Sample name	Temperature/ K	Composition analyzed by elemental analysis	Appearance[b]	
Corannulene	As received	$C_{20}H_{10}$	Yellow powder	
	773	$C_{20}H_{8.1}$	Black solid	
	823	$C_{20}H_{7.6}$	Black film	
	873	$C_{20}H_{7.2}$	Black film	
Fluoranthene	As received	$C_{16}H_{10}$	White powder	
	873	-[a]	Brown solid	
	903	$C_{16}H_{7.3}$	Black film	
	923	$C_{16}H_{7.1}$	Black film	
Coronene	As received	$C_{24}H_{12}$	Yellow powder	
	823	-[a]	Brown solid	
	873	-[a]	Black solid	
	923	$C_{24}H_{7.2}$	Black film	
Fullerene	As received	C_{60}	Black powder	
	1073	C_{60}	Black powder	
	1173	C_{60}	Black powder	

[a]These values could not be obtained because samples attached well to ampoules

[b]Brown/black solid indicates that raw materials in the form of powder were fused together and either brown/black powder or agglomerated materials were formed. On the other hand, black film indicates that film-like carbon materials were coated inside the wall of ampoules

hand, the C=C bond length between the carbon atom at the DUO position and the other carbon atom at the valley position of corannulene was 0.1448 nm (Fig. 4a1), which is much longer than the bond length of C=C in graphite. The long C=C bond in corannulene is related to the loss of conjugated systems between the carbon atom at the DUO position and the carbon atom at the valley position. The loss of conjugated systems at DUO positions of corannulene (Fig. 4b1) relates to the high reactivity according to the Clar's rule [64, 65], whereas the loss of conjugated systems at DUO positions of coronene was not observed (Fig. 4b4). Conjugated systems were not maintained in case of fluoranthene in a similar manner as corannulene, but the bond length of C=C at DUO positions of corannulene was longer than that of fluoranthene. The order of reactivities was estimated computationally by Martin et al. [67], and

Figure 4 Bond length of C–C and molecular orbital of raw materials. **a** Bond length. **b** Molecular orbital. (1) Corannulene. (2) Fluoranthene. (3) Fullerene. (4) Coronene. HOMO, Highest Occupied Molecular Orbital. NHOMO, Next Highest Occupied Molecular Orbital. The numbers in parentheses mean the number of each orbital.
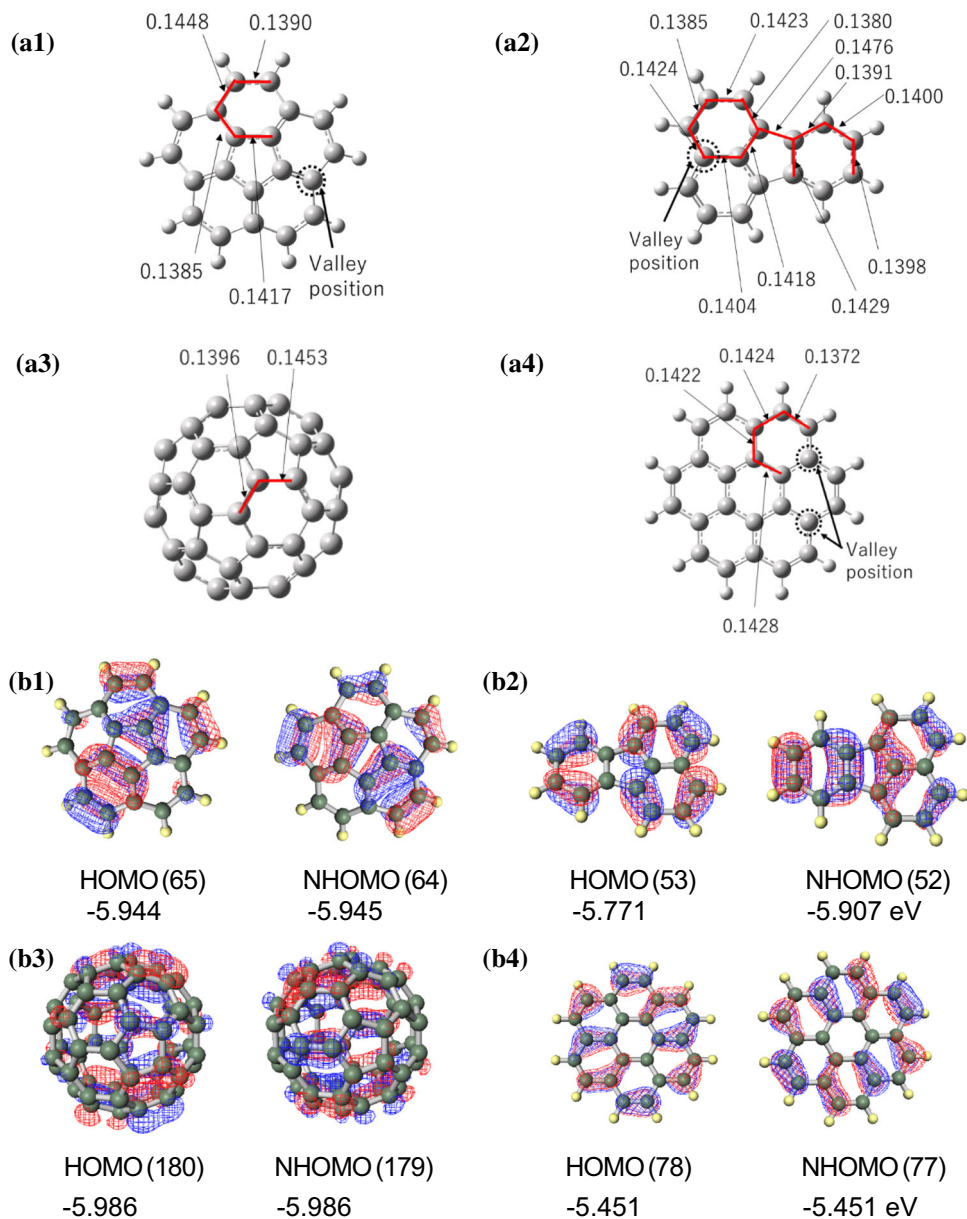
corannulene was estimated to show higher reactivity than coronene from the point of view of ionization potential and also the Clar's rule because corannulene shows the lower aromaticity than coronene. According to Martin et al. [67], the reactivity can be further enhanced by introducing pentagons on edges, such as acenaphthylene, rather than pentagons confined in the basal plane, but those pentagons on edges possibly form decacyclene-like structures rather than corannulene-like structures after carbonization according to the summary by Mochida et al. [36]. Fullerene, on the other hand, did not show high reactivity during carbonization. This is because of the difficulty to form carbon radicals by scission of

the C=C bond. By calculation, optimization of structures of fullerene with cleaved C=C bonding with two radicals was conducted, but the cleaved C=C bond was healed during the optimization, and C=C bond was formed. Thus, the scission of the C=C bond in fullerene hardly occurred because the cleaved C=C bond rejoined in the presence of the ball-like stable structure.

The structural stability of corannulene with curvature was further investigated. Two types of structures of corannulene with and without curvature could be obtained after optimization of corannulene. The energy after optimization of corannulene with curvature was 0.38 eV lower than that without

curvature in terms of total electron energy. As shown later, as the molecular weight of dehydrogenated corannulene increased, the removal of the curvature from dehydrogenated corannulene became difficult because pentagons are stable with curvature [41] unlike mixed defects of pentagons and heptagons without curvature such as grain boundary and Stone-Thrower-Wales defects [42].

From the viewpoint of energies required for the formation of the PAH radical and the hydroxy radical, the formation energy of the corannulene radical was the lowest (5.063 eV in Fig. 5) among all the formation energies of PAH radicals of raw materials. The lowest formation energy of the fluoranthene radical (5.085 eV) was smaller than that of coronene radical (5.102 eV), whereas the highest formation energy of the fluoranthene radical (5.113 eV) exceeded that of the coronene radical. The order of the formation energies or radicals supports the results of the lowest carbonization temperature of corannulene and the similar carbonization temperature of fluoranthene and coronene. However, the formation energies of radicals were close to each other and the reactivity during carbonization cannot be explained only by the formation energies. Thus, the high reactivity of corannulene compared to other raw materials originates from the presence of reactive C–H in corannulene, which can be easily radicalized, from the viewpoint of the formation energy and the loss of conjugated states according to Clar's rule.

MD simulation

Figure 6 shows reaction routes of (a) corannulene, (b) fluoranthene, (c) coronene, and (d) fullerene observed after being heated at a constant temperature of 3000 K in ReaxFF simulation. 3000 K was used because the reaction did not proceed at 2000 K or lower within a week of calculation and our previous studies showed the validity of calculation at 3000 K [11, 51]. Nest-like structures at the top of each figure (Fig. 6a–d) show randomly arranged molecules before heat treatment. Structures of corannulenes heated for 70 ps are shown at the bottom of Fig. 6a. At 54% conversion of corannulenes, meaning that 54% of corannulene changed into other structures, 24% of corannulenes among reacted corannulenes was dehydrogenated and up to four corannulene molecules were integrated into one molecule, and 19% was partially pyrolyzed, and formed benzo(ghi)fluoranthene-like structures. The pyrolysis was caused because of the scission of C=C bond by the energy of heat and also hydrogenation. Also, 53% of corannulene became radicalized corannulene, which can easily bond with other radicalized corannulene, and 4% of corannulene became hydrogenated corannulene, which can cause the loss of pentagons in carbon materials. Comparing the conversions of four raw materials (Fig. 6a–d), the conversion of corannulene was the highest after heat treatment for 70 ps, which can also explain the experimental results of the lowest dehydrogenation temperature of corannulene from elemental analysis (Table 1).

Heat treatment of corannulenes was further continued at a constant temperature of 3000 K until the conversion reached 100% (Fig. 6a). At 100% conversion (400 ps), most of the corannulenes were polymerized into larger chain molecules. Compared to fluoranthene heated for 400 ps, corannulene heated for 400 ps was polymerized significantly. This is because the formation of both benzo(ghi)fluoranthene-like structures and fluoranthene-like structures (Structures III and IV in Fig. 6a) accompanied with the formation of the reactive non-cyclic chain, such as ethynyl- and vinyl-like groups and acetylene chains, by the scission of C=C of hexagons in corannulene. The reactive groups accelerated the polymerization. The high reactivities of ethynyl groups, vinyl groups, and acetylene chains have been explained in previous studies [10, 48]. It has been reported that embedded-pentagons migrate to the edge by isomerization during either carbonization or the scission of C=C in pentagons proceeds [68–70]. Such pentagonal edges [67] have high reactivity as mentioned earlier. Similar results of embedded-ring migration of pentagons (Structure I in Fig. 6a) were also observed in our results of ReaxFF, although only a few structures were observed. Scissions of C=C bond of hexagons proceeded mainly as one of pyrolysis routes during 400 ps of heat treatment, and after the scission of hexagons, scissions of C=C bond of pentagons further proceeded (Structure II in Fig. 6a). Thus, these two factors such as embedded-ring migration and the scission of C=C could be the causes for pentagons to be removed upon carbonization as observed in the experimental results of Raman and XPS spectra, which will be explained later.

Carbonization reactions of fluoranthene were also simulated (Fig. 6b) under the same conditions as that of corannulene (Fig. 6a). The selectivity to

Figure 5 Formation energies of radicals. **a** Corannulene radical. **b** Fluoranthene radical. **c** Coronene radical. The numbers in parenthesis indicate the formation energies of radicals. The formation energies were calculated using Eq. 1 in experimental section. White sphere: Hydrogen atom. Gray sphere: Carbon atom.
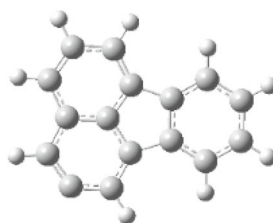
(a) Corannulene radical (5.063 eV)
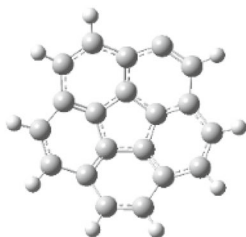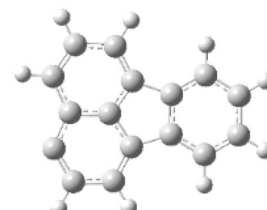

(b) Fluoranthene radical
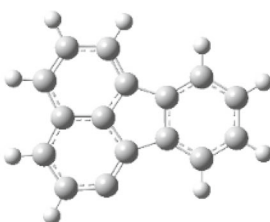
Position 1 (5.091 eV)   2 (5.085 eV)   3 (5.113 eV)
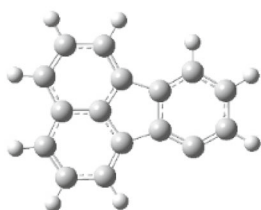
Position 7 (5.088 eV)   8 (5.101 eV)
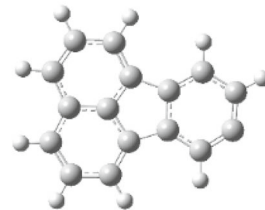
(c) Coronene radical (5.102 eV)
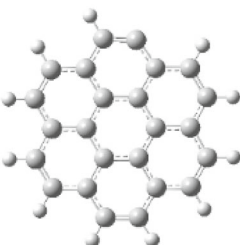
dehydrogenated structures of fluoranthene (20%) was close to those of corannulene (24%). At 50% conversion (70 ps), 73% of fluoranthene became radicalized fluoranthene monomers. One out of three benzene rings surrounding one pentagon was broken, causing pyrolysis of 7% of fluoranthene. Once one of hexagonal rings is broken, pentagons should be more susceptible to react, implying that the

pentagon in corannulene is more stable than that in fluoranthene. In a similar way to the pentagon in corannulene, the pentagon in fluoranthene was also removed by heat treatment in ReaxFF mainly because of the scission of C=C (Structure I in Fig. 6b), although most pentagons remained even after 400 ps of heat treatment. It is because the conversion of fluoranthene (88%) was lower than that of

(a) Reaction routes of corannulene

100 molecules of corannulene

At 70 ps (conversion of 54%)

Hydrogenated (Selectivity of 4%)

Radicalized (53%)

Dehydrogenated (24%)

Pyrolyzed (19%)

At 400 ps (conversion of 100%)

Structure I

(Ring migration)

II

(Loss of pentagon by scission of C=C)

III

IV
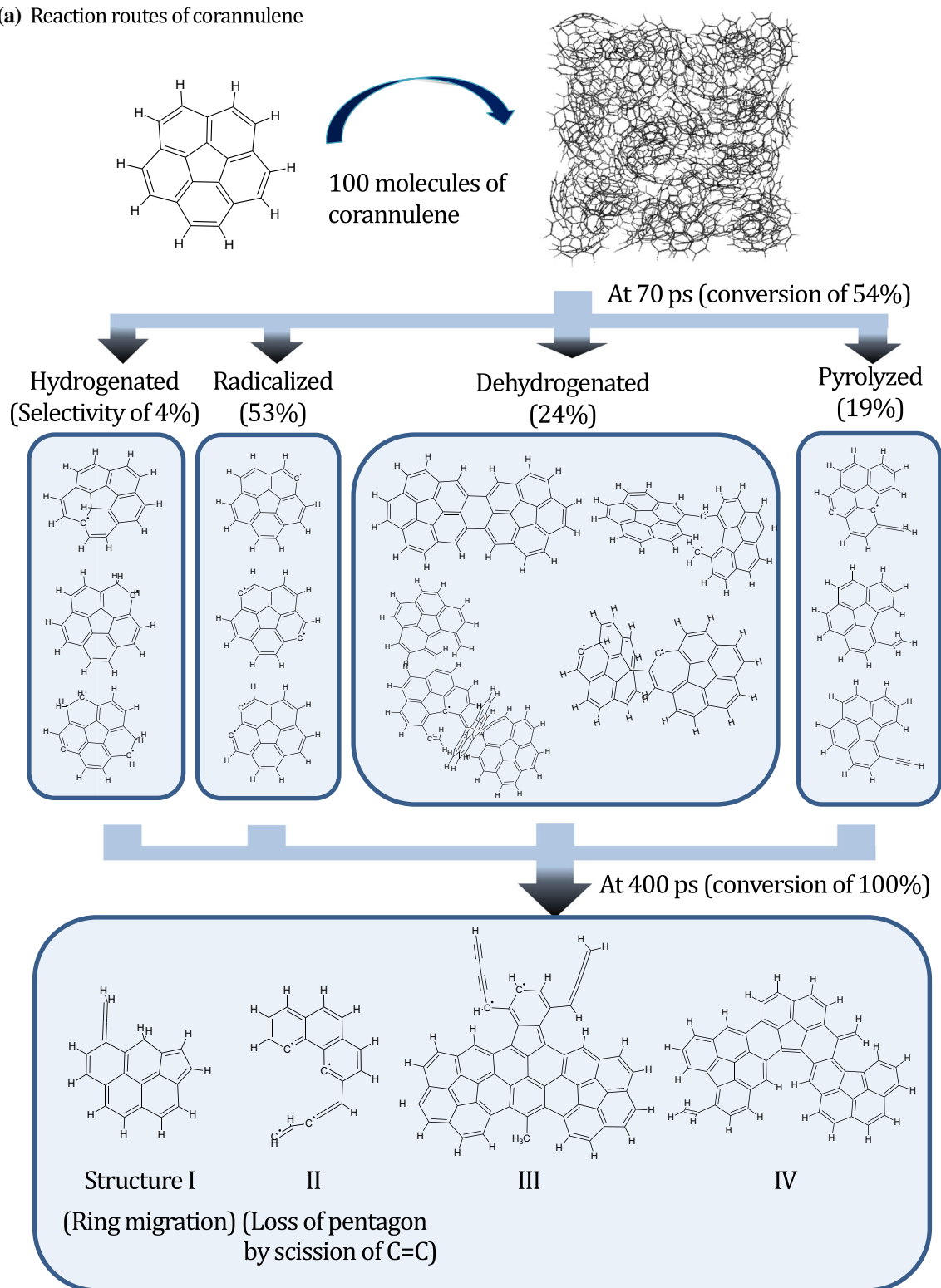
Figure 6 Reaction routes of **a** corannulene, **b** fluoranthene, **c** coronene, and **d** fullerene after heat treatment at 3000 K by ReaxFF.

(b) Reaction routes of fluoranthene

b-1) Heat treatment of fluoranthene

Figure 6 continued.

(c) Reaction routes of coronene

c-1) Heat treatment of coronene

100 molecules of fluoranthene

At 70 ps (Conversion of 46%)

Dehydrogenated (Selectivity of 18%)   Radicalized (82%)
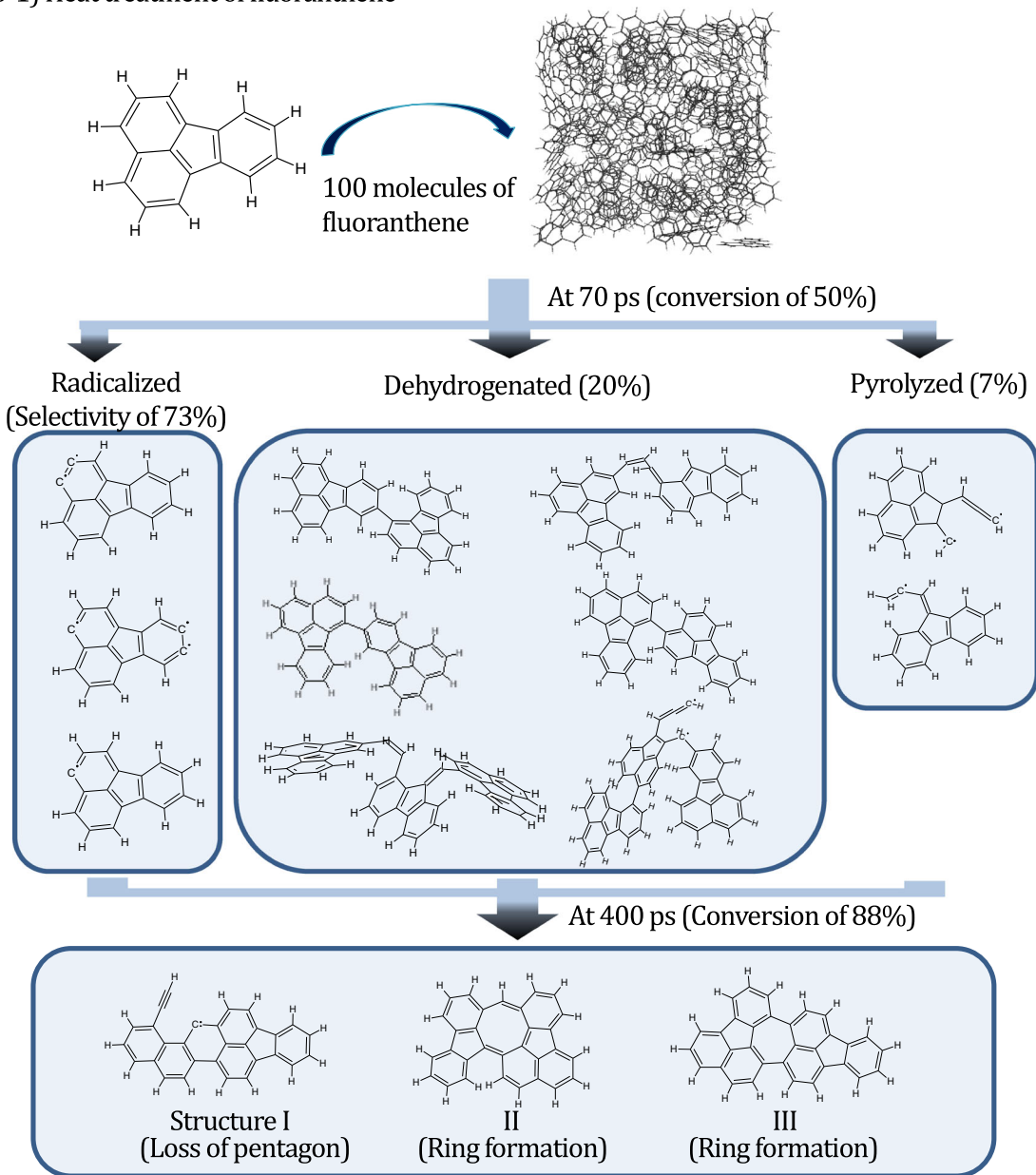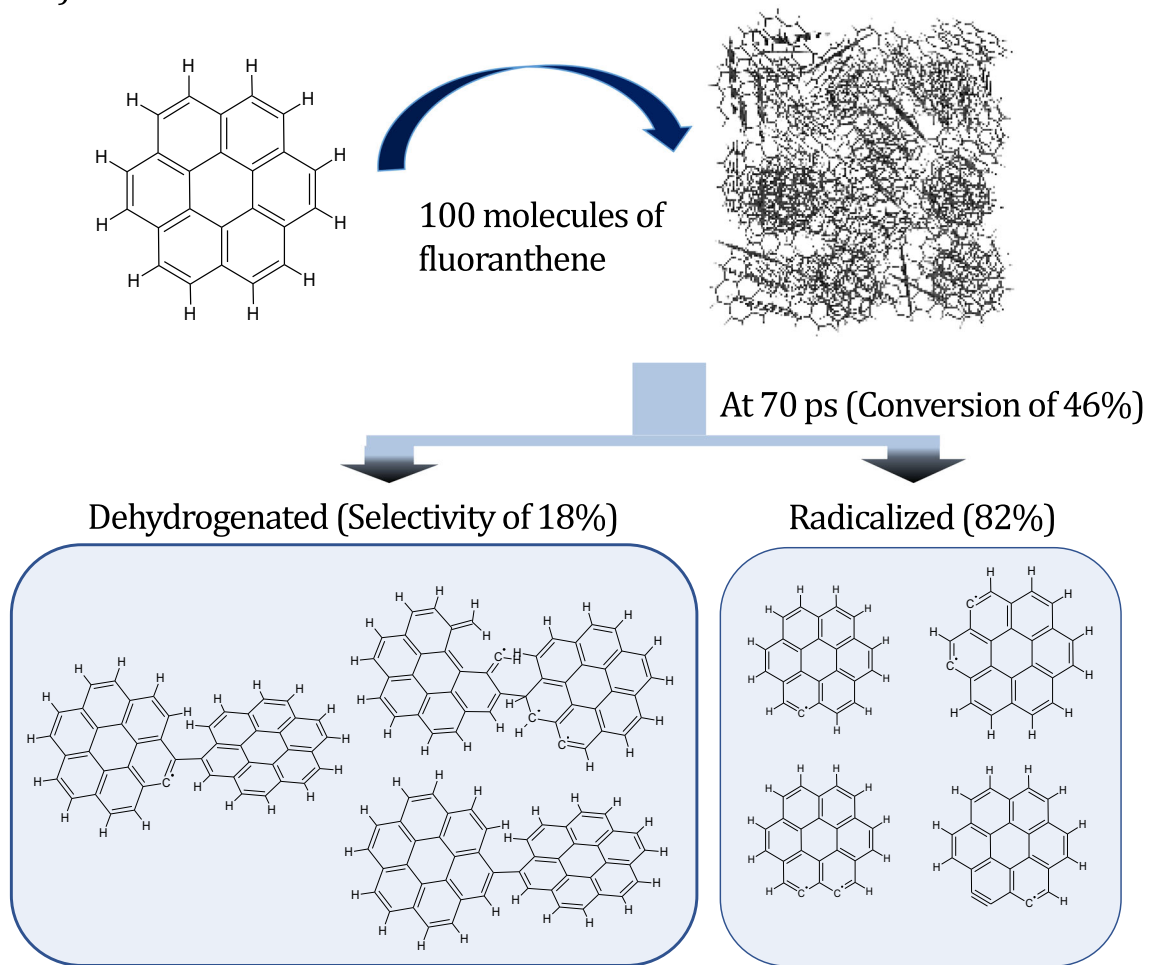
c-2) Further heat treatment at 250 ps

(Dehydrogenated structures in c-1 were further heated.)
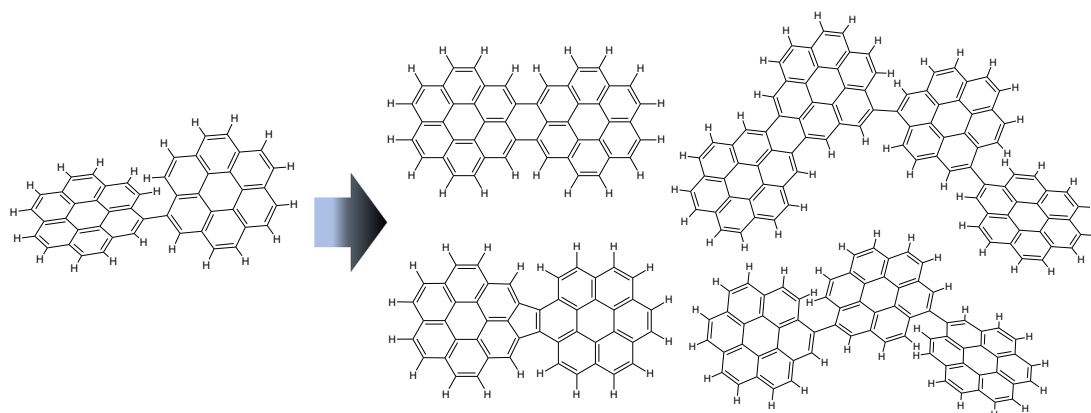
Figure 6 continued.

Figure 6 continued.

(d) Reaction route of fullerene

35 molecules of fullerenes

At 70 ps (Conversion of 11%)

C-C coupled (Selectivity of 100%)
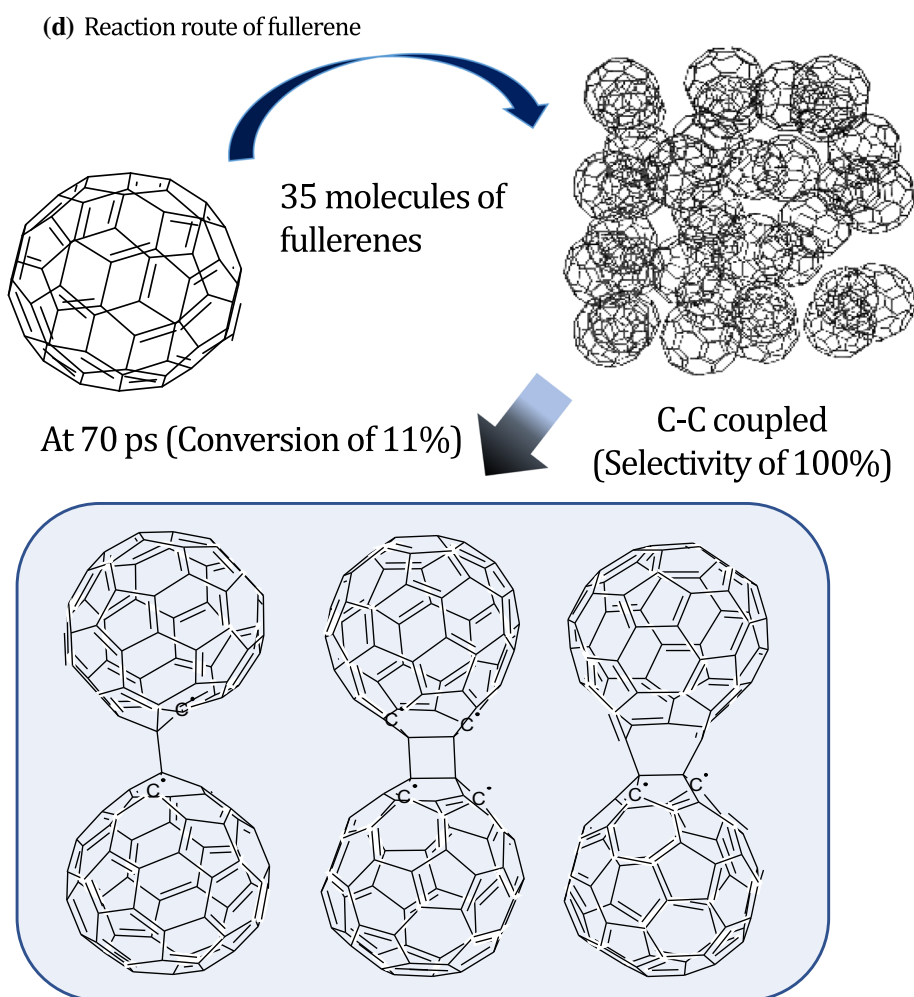
corannulene at 400 ps of heat treatment (100%) and also because the number of reactive non-cyclic chains formed from one molecule of corannulene is more than that of fluoranthene.

Reaction routes of coronene and fullerene are shown in Fig. 6c, d, respectively. These raw materials showed almost 0% of pyrolyzed molecules, implying that the low reactivity and the high thermal stability of both coronene with hexagons and hydrogen and fullerene with pentagons without hydrogen as shown in Table 1. At 70 ps of the simulation, 46% of coronene monomers reacted, and radicalized coronene molecules and dehydrogenated coronene dimers formed, while only 11% of fullerenes reacted, indicating that the reactivity of fullerene was the lowest among the raw materials. The formation of dimerized coronene upon heat treatment has been confirmed experimentally by our group [52] and another group [71]. The formation of dimer and trimer of fullerene has been reported [72, 73] in addition to the direct observation of dimerization inside carbon nanotube by transmission electron microscopy from other groups [74]. The results of ReaxFF of coronene obtained in this work also showed dimer structures with either hexagons or pentagons (Fig. 6c-2). Thus, calculated structures of dimerized coronene, further carbonized coronene, and fullerene dimers in this work are possible structures and the validity of calculated results could be confirmed. The further validations by comparing experimental spectra with calculated ones are explained in the following section.

DRIFT spectra

Experimental DRIFT spectra and calculated IR spectra of four raw materials and their carbonized samples (Figs. 7, 8, 9, 10) and the peak assignments obtained by comparing experimental and calculated spectra are shown in Table 2. Cora1 is a raw material
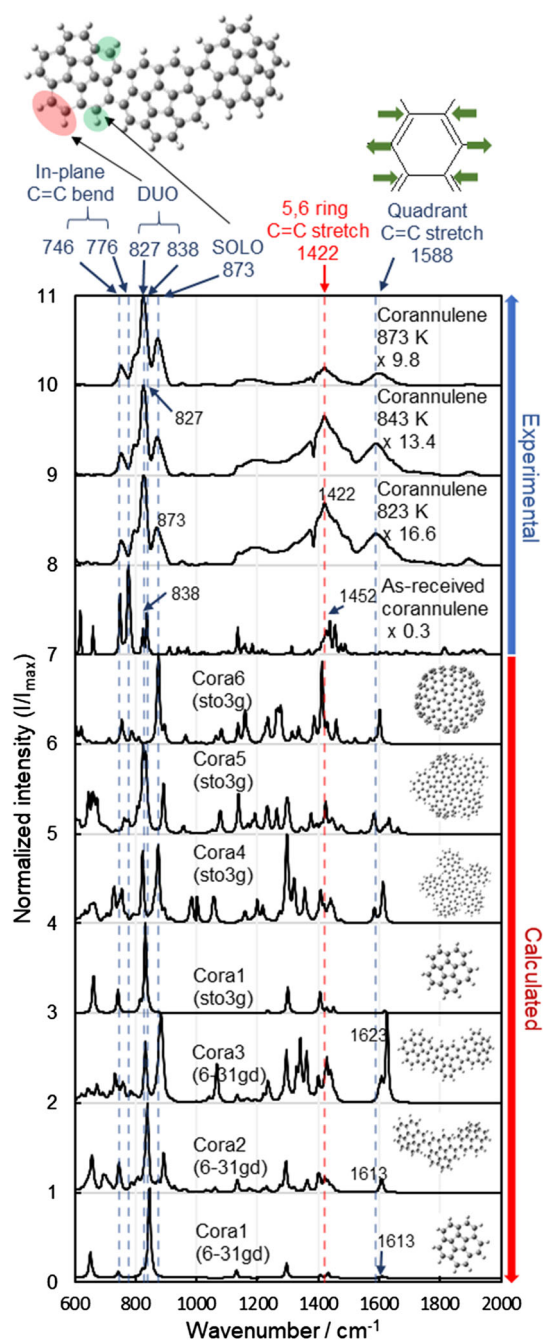
Figure 7 Calculated and experimental DRIFT spectra of as-received corannulene and corannulene heated at different temperatures. Multiplied numbers shown at the right side of experimental spectra are the numbers that multiplied to adjust the maximum intensity to be 1. Vibrations shown at the top of this figure are examples of vibrations. Other similar vibrations at different directions were also observed.

of corannulene. Cora2 is a dehydrogenated trimer of corannulene. Cora3–6 are further dehydrogenated trimer and hexamer of coronene by forming

hexagonal rings among the raw materials. Similarly, structures of fluoranthene (Fluo1), dehydrogenated fluoranthene (Fluo2–12), fullerene (Full1), fullerene dimer (Full2), coronene (Coro1), and dehydrogenated coronene (Coro2–8) were also constructed.

Calculated spectra of corannulene (Cora1), dehydrogenated corannulene (Cora2), and the further dehydrogenated corannulene (Cora3–6) and experimental spectra of as-received and carbonized corannulene showed the vibrational peaks of DUO in the range between 827 and 838 cm^{-1} (Fig. 7). In addition, SOLO (armchair-like) peaks also appeared at 873 cm^{-1} in the spectra of corannulene heated at 823 K or higher. These peaks were also observed in the calculated spectra of Cora2–6. Thus, structures similar to these structures are possibly present in experimentally carbonized corannulene. A broad peak was observed in the experimental spectra of carbonized corannulene at ca. 1422 cm^{-1}. The peak was confirmed to be a vibrational peak of C=C in pentagons after the formation of C=C bonds by dehydrogenation of two corannulene as results of the calculated spectra (Cora2–6). These broad peaks originate from C=C and C–H stretch in the presence of multiple bonding states. Peaks of quadrant C=C stretch of hexagonal rings also appeared at 1588 cm^{-1} in the spectra of carbonized corannulenes.

The experimental spectrum of as-received fluoranthene shows only QUATRO and TRIO in the range between 751 and 827 cm^{-1}, as confirmed by the comparison with calculated spectrum of fluoranthene (Fluo1) (Fig. 8). At 873 K or higher, SOLO appeared at 871–877 cm^{-1}, and the experimental intensities of especially TRIO relative to that of SOLO reduced, showing that C–H at TRIO of the fluoranthene molecules dehydrogenated and C=C bonds formed upon carbonization as confirmed by the comparison with calculated spectra of plausible structures of dehydrogenated fluoranthene. The experimental peak intensity of QUATRO relative to other peak intensities also slightly decreased, but the relative intensity of QUATRO remained high compared to those of TRIO, implying that C–H at TRIO reacted more than that at QUATRO. The low symmetry of fluoranthene allows for various reaction routes and clarification of carbonization steps is not straight forward. However, from the experimental IR spectra compared to calculated IR spectra, the mainly reacted positions could be estimated. The presence of pentagons was confirmed at 1455 cm^{-1} for as-received
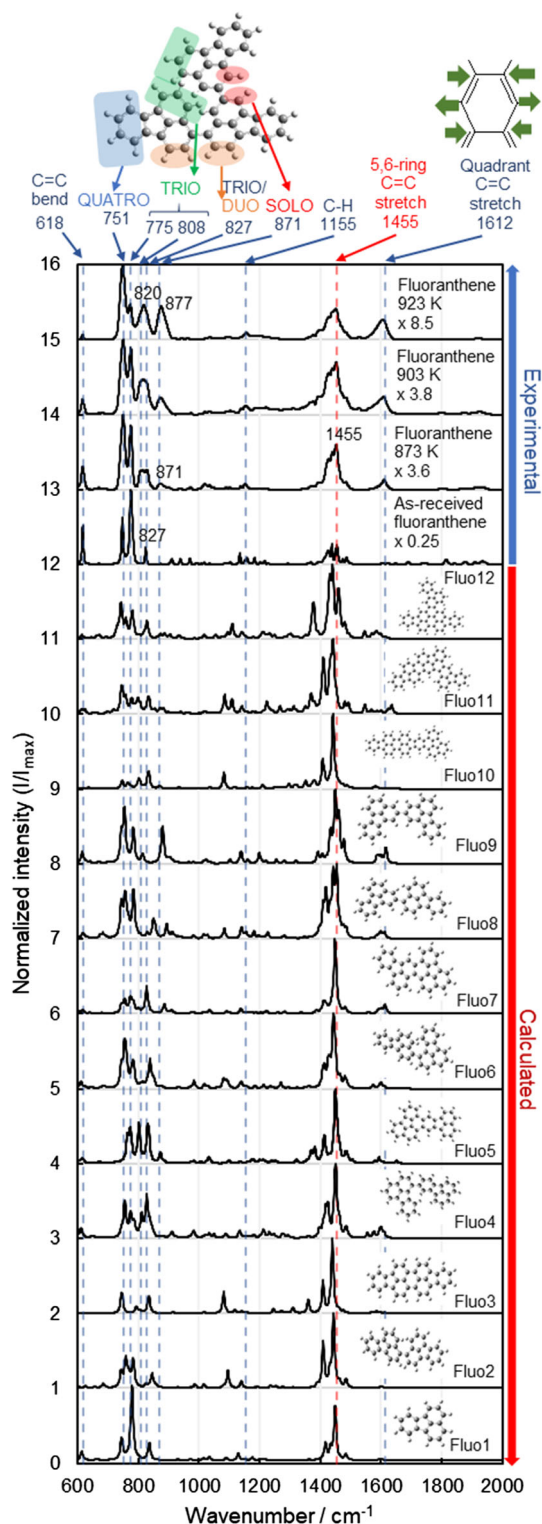
Figure 8 Calculated and experimental DRIFT spectra of as-received fluoranthene and fluoranthene heated at different temperatures. Multiplied numbers shown at the right side of experimental spectra are the numbers that multiplied to adjust the maximum intensity to be 1. Vibrations shown at the top of this figure are examples of vibrations. Other similar vibrations at different directions were also observed.
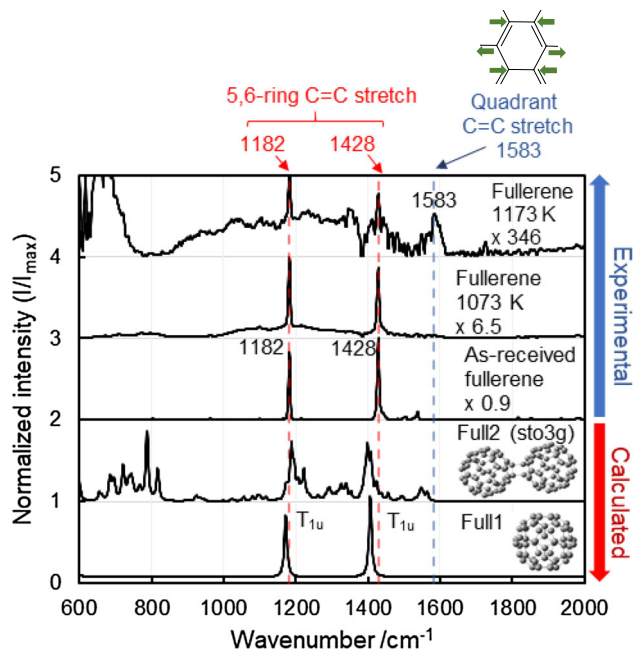
Figure 9 Calculated and experimental DRIFT spectra of as-received fullerene and fullerene heated at different temperatures. Multiplied numbers shown at the left side of experimental spectra are the numbers that multiplied to adjust the maximum intensity to be 1. Vibrations shown at the top of this figure are examples of vibrations. Other similar vibrations at different directions were also observed.

and carbonized fluoranthene. In addition, a peak derived from the quadrant stretching vibration of C=C in hexagonal rings of the polymerized fluoranthene was clearly observed at 1612 cm^{-1} in carbonized fluoranthene. The presence of various structures of carbonized fluoranthene is possible because of the broad FWHM of experimental peaks compared to the calculated ones, but especially the calculated spectra of Fluo9 and Fluo12 were close to the experimental spectra of carbonized fluoranthene among calculated spectra.

The experimental spectra of as-received fullerene and fullerene heated at 1173 K showed strong peaks at 1182 and 1428 cm^{-1} because of the presence of pentagons (Fig. 9), which relate to the T1u symmetry [75]. At 1173 K, fullerene was either dimerized or polymerized to a certain extent, which can be explained by the decrement of peak intensities related to pentagons at 1182 and 1428 cm^{-1}, and the increment of the relative peak intensity at 1583 cm^{-1}, which originates from quadrant stretching vibration of C=C in hexagonal rings. The experimental spectra of as-received fullerene and fullerene heated at

Figure 10 Calculated and experimental DRIFT spectra of as-received coronene and coronene heated at different temperatures. Multiplied numbers shown at the right side of experimental spectra are the numbers that multiplied to adjust the maximum intensity to be 1. Vibrations shown at the top of this figure are examples of vibrations. Other similar vibrations at different directions were also observed.
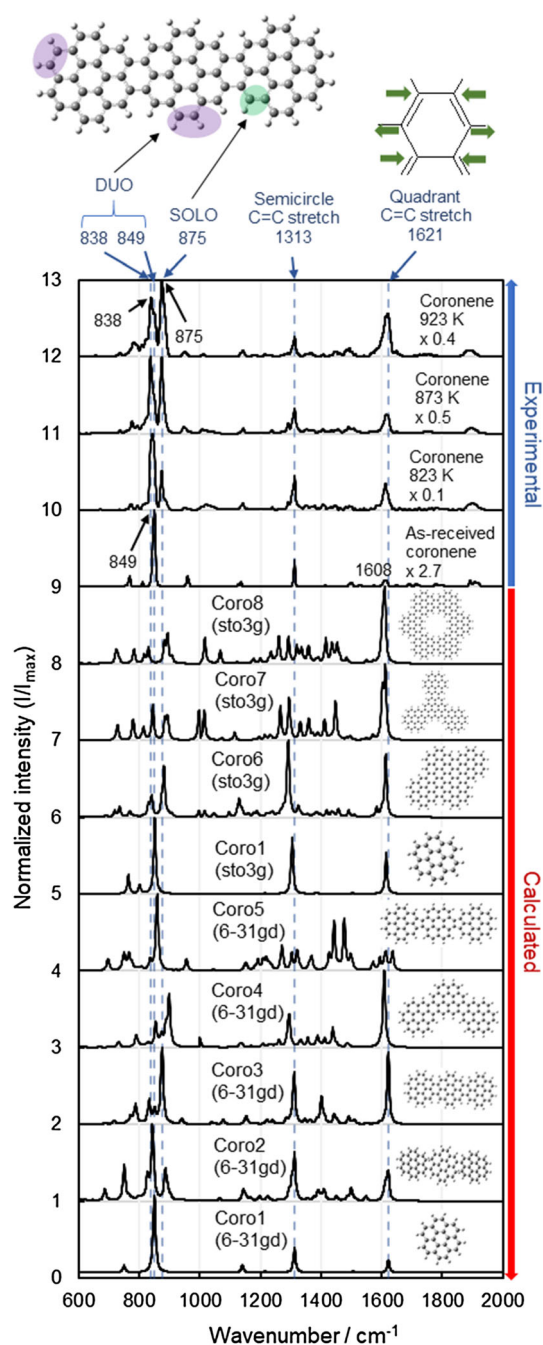
1173 K were close to those of calculated spectra of fullerene (Full1) and fullerenes bonded together

(Full2). However, fullerene did not form a film even at 1173 K (Table 1), because of the low reactivity.

Experimental IR spectrum of as-received coronene showed no clear sign of the peak of pentagons ranging from 1422 (for carbonized corannulene) to 1455 (for carbonized fluoranthene) cm^{-1} (Fig. 10), as discussed in our previous work [52]. Hence, pentagons were either absent or present at a low percentage in the carbonization of coronene. After carbonization at 923 K, experimental peaks originating from DUO and SOLO of dehydrogenated coronene (Coro2, 3, and 6) appeared at 838 and 875 cm^{-1}. Thus, the structures similar to Coro2, 3, and 6 are possibly present.

Raman spectra

Raman spectroscopy has been generally utilized to analyze defects in carbon materials such as edges, pentagon, heptagon, and functional groups. Peaks at ca. 1580–1600 cm^{-1} are well known as a G band derived from the C=C stretching vibration of hexagonal aromatic rings [53, 55, 56], whose C=C stretch vibration is called as quadrant stretch [11]. In addition, G band influenced by defects, such as edges, shifts peak positions higher at 1600–1650 cm^{-1}, which is also called as D′ band [54]. These vibration modes of G and D′ bands are similar, and both vibrations are categorized as quadrant stretch. The D band, known as a disordered band, appears in the presence of defects other than the basal plane with hexagonal aromatic rings [11, 54].

Experimental and calculated Raman spectra of four raw materials and their carbonized samples (Figs. 11, 12, 13, 14) in addition to their assignments of peaks are shown in Table 3. Figure 11 shows the experimental Raman spectra of as-received and heat-treated corannulene and the calculated Raman spectra of predicted structures of carbonized corannulene. Experimental peaks of as-received corannulene appeared at 1430 and 1627 cm^{-1}, which originate from the presence of pentagons and D′ band (quadrant stretch), respectively. After carbonization of corannulene, the peak originated from pentagons at 1430 cm^{-1} shifted in the range between 1452 and 1462 cm^{-1}, while D′ band at 1627 cm^{-1} shifted in the range between 1592 and 1600 cm^{-1}, and the peak position became closer to G band. The peak shift from 1430 cm^{-1} (pentagon) to 1462 cm^{-1} is caused by the formation of C=C coupling (Cora2) and the formation

Table 2 Assignment of experimental peak positions of IR spectra estimated by calculated IR spectra

Wavenumber/cm^{-1}	Type of vibration
1621	D′-band like/Quadrant C=C stretch (Carbonized coronene)
1612	D′-band like/Quadrant C=C stretch (Carbonized fluoranthene)
1588	G-band like/Quadrant C=C stretch (Carbonized corannulene)
1583	G-band like/Quadrant C=C stretch (Polymerized fullerene)
1455	5,6 ring C=C stretch (Fluoranthene/Carbonized fluoranthene)
1428	Fullerene (T1u)
1422	5,6 ring C=C stretch (Corannulene/Carbonized corannulene)
1313	D-band like/Semicircle C=C stretch (Coronene/Carbonized coronene)
1182	Fullerene (T1u)
875	SOLO (Carbonized coronene)
873	SOLO (Carbonized corannulene)
871	SOLO (Carbonized fluoranthene)
838–849	DUO (Coronene/ Carbonized coronene)
827–838	DUO (Carbonized corannulene)
775–827	TRIO/DUO (Fluoranthene/Carbonized fluoranthene)
746–776	C=C in-plane bend (Corannulene/Carbonized corannulene)
751	QUATRO (Fluoranthene/Carbonized fluoranthene)

of new hexagons via the dehydrogenation between corannulene molecules (Cora3-6). The lower peak shift of D′ band is caused by the decrement of edges by the dehydrogenation [11, 45]. After carbonization at 823–873 K, new sharp peaks were observed at 1182–1183 and 1285–1287 cm^{-1} corresponding to C–H bending and C=C breathing, respectively, indicating that dehydrogenation such as Cora3 without decomposition of corannulene structures clearly proceeded. These peak positions, including a part of the peak derived from pentagons, are generally categorized as D band in Raman spectra of general carbon materials. Although the calculated Raman spectrum of the structure of Cora3 was the closest to the experimental Raman spectra of corannulene at 873 K, it is possible that other structures with higher molecular weight similar to Cora4-6 are mixed, because the experimental peak positions of corannulene at 923 and 943 K were quite different from those at 823–873 K.

Experimental and calculated Raman spectra of as-received and carbonized fluoranthene are shown in Fig. 12. The experimental peaks of fluoranthene at 1413 and 1457 cm^{-1} originate from the presence of pentagons. After carbonization at 873–923 K, the experimental peaks at 1413 and 1457 cm^{-1} shifted to 1390–1392, 1432, and 1454–1459 cm^{-1}. These peaks were clearly observed in the calculated spectrum of Fluo3, Fluo10, and Fluo12. Strong peaks at 1282–1285 cm^{-1} of carbonized fluoranthene are derived from in-plane C–H bending on armchair edges with C=C breathing and C=C stretching. C–H groups on armchair edges can be formed by dehydrogenation at position 2 (Fluo4, Fluo8, and Fluo9) and position 3 (Fluo2, Fluo3, Fluo6-8, and Fluo10-12) (Figs. 1aii and 12). In a similar way to FWHMs of IR spectra, those of calculated Raman spectra were much larger, indicating that various structures should be mixed due to the low symmetry compared to other raw materials. Especially, the calculated Raman spectra of Fluo3, Fluo9, and Fluo10–12 were close to experimental spectra of carbonized fluoranthene. Calculated IR spectra of Fluo9 and Fluo12 were also close to the experimental IR spectra. Thus, structures close to those structures (Fluo9 and Fluo12) are expected to form as results of Raman and IR spectra.

Experimental and calculated Raman spectra of as-received and heat-treated fullerene are shown in Fig. 13. The Raman spectra of heat-treated fullerene deposited on the inner wall of ampoules and heat-treated powdery fullerene without deposition on the inner wall at 1173 and 1093 K were separately analyzed. Experimental Raman spectra of as-received and heat-treated fullerene showed strong peaks at 1471–1463 cm^{-1}, which attribute to the vibration of C=C influenced by the presence of pentagons. As shown in Table 1, the appearance of fullerene remained as black powder even after being heated at 1173 K. Thus, the peak positions of heat-treated
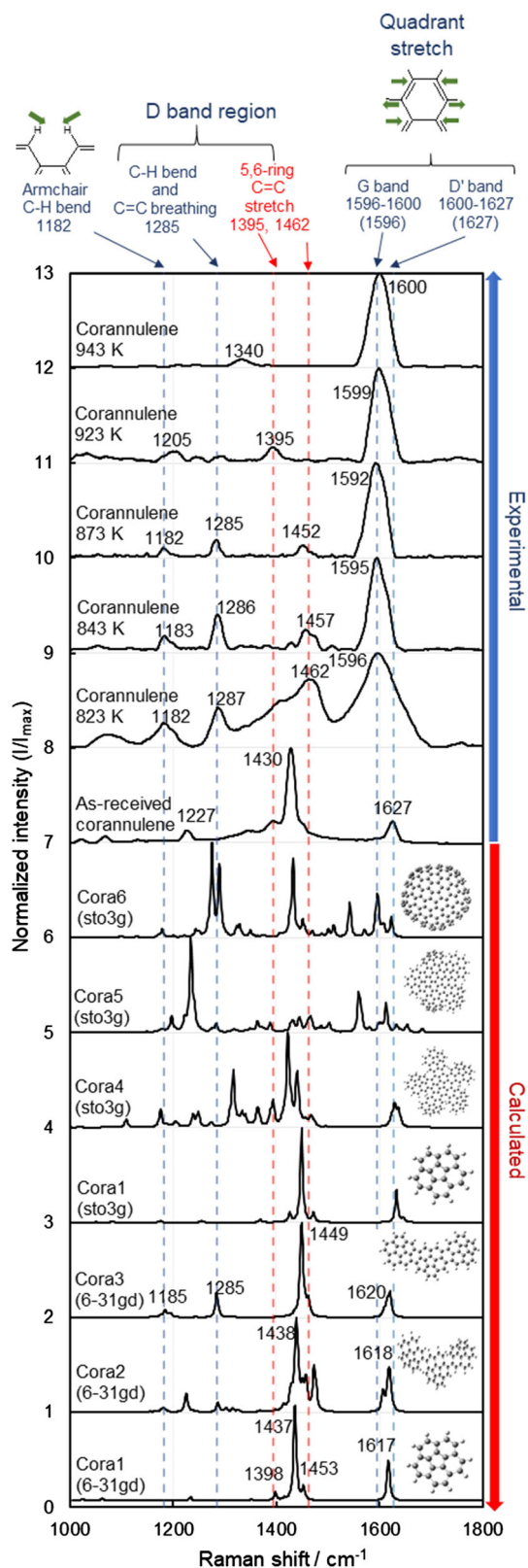
◀ **Figure 11** Calculated and experimental Raman spectra of as-received and heated corannulene at different temperatures. Vibrations shown at the top of this figure are examples of vibrations. Other similar vibrations at different directions were also observed.

fullerene at 1463–1466 cm^{-1} at 1073 and 1173 K were slightly lower than that of as-received fullerene (1471 cm^{-1}), because of the presence of the reacted fullerene (Full2 in Fig. 13). The sample deposited on the inner wall at 1073 K showed low intensities of peaks originated from the presence of pentagons at 1465 cm^{-1} and showed wide FWHM of D band at 1400 cm^{-1} (Fig. 13), implying that the percentage of pentagons decreased.

Experimental Raman spectra of as-received coronene and coronene heated at 873 and 923 K are shown in Fig. 14. Calculated Raman spectra of coronene and possible structures of heat-treated coronene are also shown in Fig. 14. No peak related to pentagons was observed in the range between 1392 (carbonized fluoranthene) and 1471 (fullerene) cm^{-1} in the experimental spectrum of as-received coronene. Experimental peaks at 1351 and 1368 cm^{-1} of as-received coronene shifted to 1325, 1349, and 1406 cm^{-1} after carbonizing coronene at 923 K. This shift to 1325 cm^{-1} is associated with the formation of graphene-like structure (Coro6), and the shift to 1349 cm^{-1} is associated with the formation of either dehydrogenated structure (Coro2) or hexagons (Coro3, 4, 7, and 8). The presence of the experimental peak at 1406 cm^{-1} is possibly related to the presence of pentagons (Coro5) because the formation of pentagons between coronene molecules was observed by heat treatment in ReaxFF (Fig. 6c2), but the presence of pentagon was obscured because clear peaks could not be observed as results of experimental IR spectrum of carbonized coronene compared with the calculated spectrum of Coro5 in Fig. 10. Experimental peaks at 1586, 1607, and 1620 cm^{-1} were clearly observed in the spectrum of coronene at 923 K. These sharp peaks can be explained by the presence of different types of bonding states between coronene molecules. The high symmetry of coronene generated sharp peaks even after the heat treatment in opposition to broad peaks of Raman spectra of general carbon materials. The peak of D′ band at 1620 cm^{-1} is related to coronene (Coro1) and coronene bonded with another coronene by forming one C=C bonding
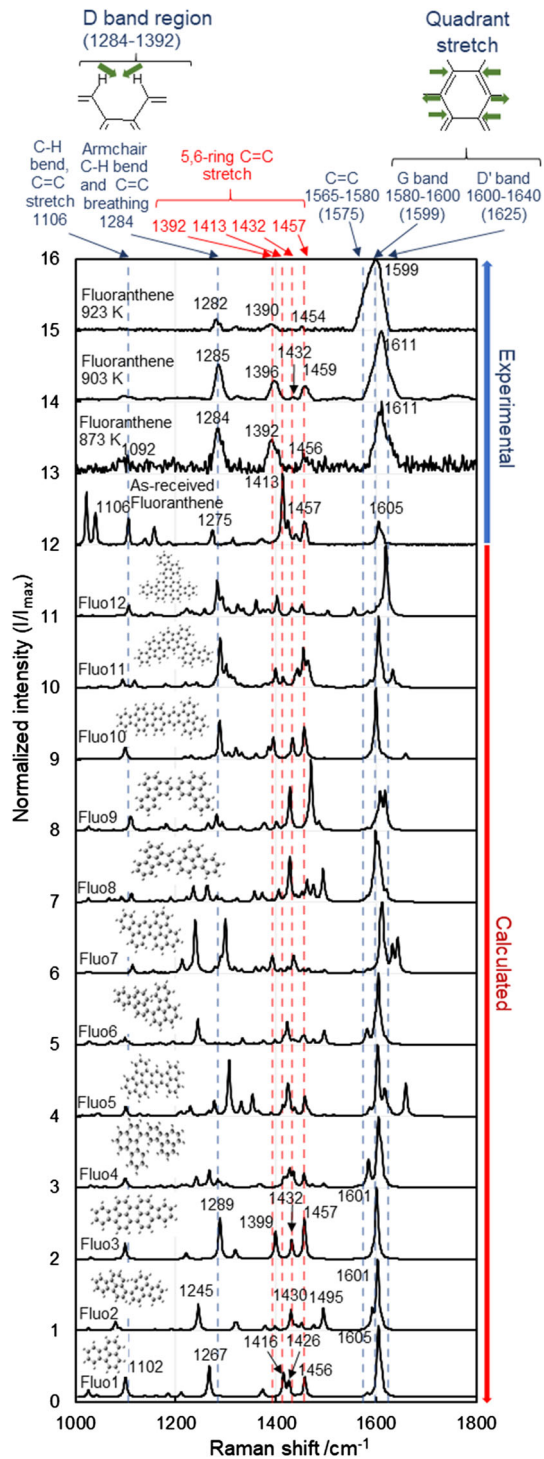
Figure 12 Experimental and calculated Raman spectra of as-received and heat-treated fluoranthene at different temperatures. Vibrations shown at the top of this figure are examples of vibrations Other similar vibrations at different directions were also observed.
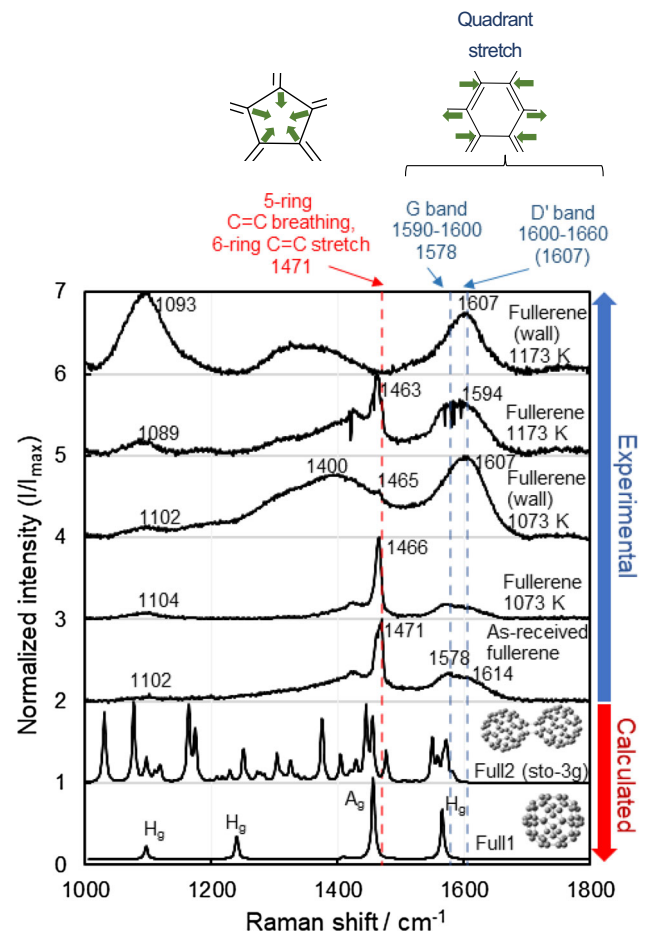
Figure 13 Experimental and calculated Raman spectra of as-received and heat-treated fullerene at different temperatures. Vibrations shown at the top of this figure are examples of vibrations. Other similar vibrations at different directions were also observed. Fullerene (wall) indicates the spectrum of thermally treated fullerene attached on the wall of ampoule tubes.

(Coro2). The peak of D′ band at 1607 cm^{-1} is related to coronene bonded with another coronene by forming one C=C bonding (Coro2). The peak of G band at 1586 cm^{-1} is associated with coronene bonded with another coronene with a newly formed hexagon (Coro3, 4, and 6–8). Thus, structures such as Coro2–4, and 6–8 and the similar structures are the plausible structures after carbonization of coronene at 873–923 K. By combining the results of IR (Fig. 10) and Raman spectra (Fig. 14), the structures similar to Coro2, 3, and 6 are possibly present.

XPS spectra

Our previous studies on calculated C1s XPS spectra, such as pentagons [41] and Stone-Thrower-Wales

Figure 14 Experimental and calculated Raman spectra of as-received coronene and coronene heated at 873 and 923 K. Vibrations shown at the top of this figure are examples of vibrations. Other similar vibrations at different directions were also observed.
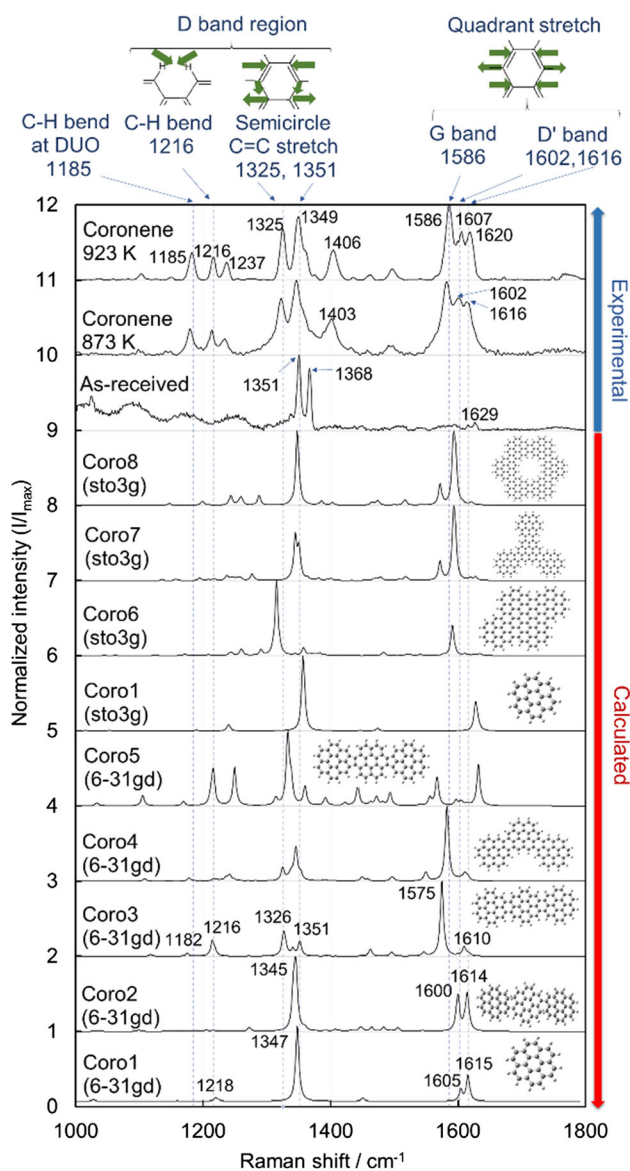
defects [42] in graphene, showed that the experimental peak positions can be estimated from calculated ones because of the high correlation between experimental and calculated peak positions [42–45]. Especially, our group has reported the importance of the FWHM of C1s spectra and the C1s peak positions of C=C in pentagons and hexagons in graphene [41]. As the number of pentagons in graphene increased from 0 to 6, the FWHM of C1s XPS spectra increased from 1.25 to 1.45 eV because of the increment of

bonding states and the different peak positions of C=C in pentagons and those in hexagons. On the other hand, as the number of pentagons in graphene increased further from 6 to12 (fullerene), the FWHM of C1s XPS spectra decreased from 1.45 to 1.15 eV because of the decrement of the number of the bonding state to 1 [41]. In addition, as the number of pentagons in graphene increased from 2 to 8, the peak positions of C=C in pentagons relative to those in hexagons approached from − 0.7 (2 pentagons) to − 0.3 (8 pentagons) eV [41]. This indicates that the peak positions of C=C in pentagons and those in hexagons can be distinguished. Thus, the C1s XPS spectra were utilized to estimate the percentage of pentagons in carbon materials. However, it should be noted that this method cannot be utilized in the presence of sp^3C and hetero atoms such as oxygen and nitrogen, because the presence of sp^3C and the hetero atoms shifts the peak positions significantly [42–44, 46].

Table 4 shows the calculated peak positions of C1s XPS for one corannulene molecule (Cora1), dehydrogenated corannulene (Cora2), and the further dehydrogenated corannulene (Cora3) (Fig. 15). As results of IR, Raman spectra, and ReaxFF (Figs. 6a, 7, and 11), corannulene molecules were dehydrogenated and new hexagons formed (Cora3 in Fig. 15) by heat treatment. Cora2 was also observed during heating as results of ReaxFF (Fig. 6c1). These structures, such as Cora2 and 3, have different degrees of dehydrogenation and are used as examples of carbonized corannulene. A comparison of calculated peak positions of C=C in pentagons, C=C in hexagon, and C–H of these three structures can be utilized to estimate the experimental ones at the different degrees of dehydrogenation. Thus, C1s spectra of these structures were simulated and applied to assign the experimental peak positions (Table 5).

Because the C=C of pentagons in corannulene was fully surrounded by hexagons, the calculated binding energy of the peak of C=C of pentagons in Coro1 (283.49 eV) was positioned much lower than those of the other characteristic peaks such as C–H (284.23 eV) and standard C=C (284.30 eV) (Table 4) unlike C=C of pentagons in fluoranthene (284.10 eV in Table 6). The calculated peak position of C=C in pentagons in Cora2 and 3 was 283.42 eV, and the calculated peak position of C=C in the newly formed hexagons in Cora3 was 248.50 eV (Table 4). Calculated peak positions of Cora1 were used to analyze

Table 3 Assignment of experimental peak positions of Raman spectra estimated by calculated Raman spectra

Raman shift/ cm^{-1}	Type of vibration
1600–1660	D′-band/ Quadrant C=C stretch (Carbonized fullerene)
1600–1640	D′-band/Quadrant C=C stretch (Carbonized fluoranthene)
1602–1629	D′-band/Quadrant C=C stretch (Coronene/Carbonized coronene)
1600–1627	D′-band/Quadrant C=C stretch (Corannulene/Carbonized corannulene)
1607	D′-band/Quadrant C=C stretch (Polymerized fullerene)
1605	D′-band/Quadrant C=C stretch (fluoranthene)
1596–1600	G-band/Quadrant C=C stretch (Carbonized corannulene)
1586	G-band/ Quadrant C=C stretch (Carbonized coronene)
1578	Hg (Fullerene)
1471	Ag (Fullerene)
1395, 1462	5,6 ring C=C stretch (Carbonized corannulene)
1413–1459	5,6 ring C=C stretch (Fluoranthene/ Carbonized fluoranthene)
1400	D-band region/C=C stretch (Polymerized fullerene)
1390–1392	D-band region/5,6 ring C=C stretch (Carbonized fluoranthene)
1325–1349	D-band region/Semicircle stretch of C=C (Carbonized coronene)
1285–1287	D-band region/C–H bending and C=C breathing (Carbonized corannulene)
1282–1285	D-band region/Armchair C–H bending and C=C breathing (Carbonized fluoranthene)
1182	Armchair C–H bending (Carbonized corannulene)
1092–1106	C–H bend, C=C stretch (Fluoranthene/Carbonized fluoranthene)
1093–1102	Hg (Fullerene/Carbonized fullerene)

Table 4 Calculated peak positions of C1s XPS spectra for corannulene (Cora1) and the dehydrogenated corannulene (Cora2), and further dehydrogenated corannulene (Cora3)

Structure	Calculated C1s peak position/eV			
	Pentagonal C=C	Hexagonal C=C	Standard C=C	C–H
Cora1	283.49	0.00	284.30	284.23
Cora2	283.42	0.00	284.30	284.17
Cora3	283.42	284.50	284.30	284.17

experimental peak positions of C1s XPS spectra of as-received corannulene (Fig. 16 and Table 5). The peak positions of C1s XPS spectra analyzed in this work were basically lower than typical peak positions of carbon materials because of the balance between utilization of neutralization and the low electrical conductivity of raw materials and quartz substrates. As observed in the experimental and calculated C1s XPS spectra of corannulene, fluoranthene, and coronene, it is clear that the peak of C=C originating from pentagon surrounded by five hexagons is present because of the largest FWHM of the total C1s

spectrum of the experimental C1s XPS spectrum of as-received corannulene among those of compared raw materials. Calculated peak positions of Cora3 were used to analyze corannulene carbonized at 823–873 K. The experimental peak positions were fixed at different carbonization temperatures between 823 and 873 K, but both the intensity and FWHM were adjusted to the experimental spectra because assignments would be unclear unless peak positions were fixed. The dehydrogenation also shifted the calculated peak position of C=C of pentagons in Cora3 (283.42 eV) to slightly lower energy
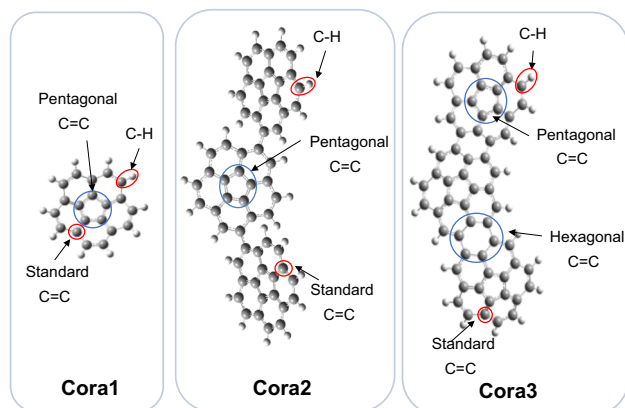
Figure 15 Structures of corannulene (Cora1), dehydrogenated corannulene (Cora2), and the further dehydrogenated corannulene (Cora3) used for assignments of C1s XPS spectra.

than that of the monomer, Cora1 (283.49 eV). Thus, dehydrogenation influences the peak positions.

The experimental FWHM of 1.46 eV of total C1s spectra of corannulenes carbonized at 843 and 873 K was larger than that of 1.44 eV of as-received corannulene. As results of calculation, FWHMs of corannulene and dehydrogenated corannulene were basically the largest among all the raw materials and the dehydrogenated raw materials. The large

FWHMs are mainly caused by the presence of pentagons surrounded by both five hexagons and C–H groups in the compound. Experimental FWHMs of carbonized corannulene remained large even at 823–873 K, indicating the presence of pentagons in the samples. These large FWHMs were not observed in experimental C1s spectra of other raw materials and the carbonized samples, as explained later. It was also confirmed that these large FWHMs were not due to the presence of functional groups (Figs. 7, 8, 9, 10, 11, 12, 13, 14 and S3–S6).

Experimental areal percentages of pentagonal C=C, hexagonal C=C, standard C=C, and C–H in as-received and heat-treated corannulenes are summarized in Table 5. The percentages of H and C obtained by elemental analysis (Table 1) were utilized to assign the experimental peaks of C–H and C=C. At the film forming temperature of 823 K, 52% of pentagons remained compared to as-received corannulene, assuming that corannulene has 100% of pentagons. The percentage of pentagons decreased with increasing temperatures (52% (823 K), 44% (843 K), and 40% (873 K)) partly because of the pyrolysis of pentagons. By assuming that the percentage of pentagon in corannulene is "one pentagon" divided by "5 hexagons and 1 pentagon", the percentage of

Table 5 Areal percentages of C=C and C–H in experimental C1s XPS spectra for as-received corannulene and corannulene heated at 823, 843, and 873 K

Structure	Areal percentage of carbon/ %				Ratio of C=C from elemental analyses[a]
	Pentagonal C=C (%)	Hexagonal C=C	Standard C=C	C–H	C=C:C–H
As-received corannulene	25 (100)	0	25	50	10:10
Corannulene 823 K[b]	13 (52)	23	23	41	–
Corannulene 843 K	11 (44)	27	24	38	12.4:7.6
Corannulene 873 K	10 (40)	28	26	36	12.8:7.2

(): Percentages in parenthesis indicate the remained percentages of pentagon in carbonized samples

[a]Results of elemental analysis are obtained from Table 1

[b]The areal percentage of carbon at 823 K was estimated using tendencies of other temperatures

Table 6 Calculated peak positions of C1s XPS spectra for fluoranthene (Fluo1), dehydrogenated fluoranthene (Fluo2), and further dehydrogenated fluoranthene (Fluo3)

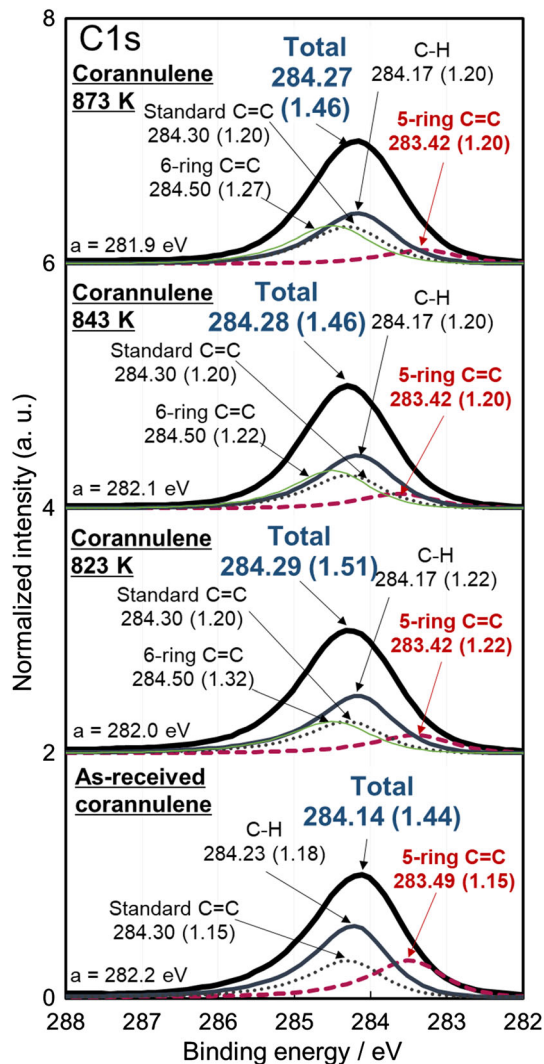| Structure	Calculated C1s peak position/eV			
	Pentagonal C=C	Hexagonal C=C	Standard C=C	C–H
Fluo1	284.10	0.00	284.30	284.17
Fluo2	283.83	0.00	284.30	283.90
Fluo3	283.90	284.30	0.00	283.96

Figure 16 Experimental C1s XPS spectra of as-received and heat-treated corannulenes. "a" in this figure represents the C1s peak position before correction of peak tops using standard C=C.

Figure 17 Structures of fluoranthene (Fluo1), dehydrogenated fluoranthene (Fluo2), and the further dehydrogenated fluoranthene (Fluo3) used for assignments of C1s XPS spectra.

symmetry among the raw materials. Thus, it is not straight forward to reveal the detailed structures of carbonized fluoranthene, but Fluo2 and Fluo3 are two possible structures because of the close experimental and calculated peak positions of especially Raman spectra (Fig. 12). Unlike the low calculated peak position of pentagons in corannulene, the calculated peak position of pentagons in fluoranthene was 284.10 eV, which is close to the peak position of C–H and almost overlapping with the peak. As mentioned above, the peak position of pentagons for C1s spectra is influenced by the surrounding environment. In the case of fluoranthene, the number of hexagons surrounding one pentagon is three, which is fewer than five hexagons of corannulene. Thus, the experimental FWHM of fluoranthene, 1.34 eV (Fig. 18), was smaller than that of corannulene, 1.44 eV (Fig. 16). Our group has reported that the FWHM increases the most as the percentage of pentagons approaches 50% because of the highest number of carbon atoms with different electron densities [41]. This study further revealed that FWHMs and peak shifts were affected by surrounding environment. It is suggested that the estimation of the percentage of pentagons in carbon materials with corannulene-like pentagons is reliable (Table 5) because the peak position of C=C in pentagons is clearly different from that in hexagons, whereas that with fluoranthene-like pentagons might not be reliable enough (Table 7) because the peak position of C=C in pentagons is close to that in hexagons. However, the percentage of pentagons is possibly underestimated using this technique, because the corannulene-like structure, which shows peaks at lower binding energy (283.4 eV), partly

pentagon becomes 17%. In that case, the percentage of pentagons decreased with increasing temperatures 8.6% (823 K), 7.3% (843 K), and 6.6% (873 K). The decrement of pentagons in the carbonized sample was also observed by experimental IR and Raman spectra because the intensities of peaks originated from pentagons became weak as the temperatures increased (Figs. 7 and 11). However, the pentagons remained at the high percentage (40% by assuming that the corannulene contains 100% of pentagons) in the sample carbonized at 873 K.

Table 6 shows the calculated C1s peak positions of fluoranthene (Fluo1), dehydrogenated fluoranthene (Fluo2), and further dehydrogenated fluoranthene (Fluo3) (Fig. 17). Fluoranthene has the lowest
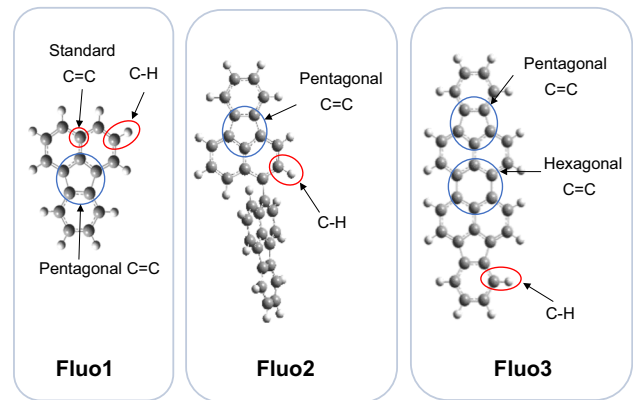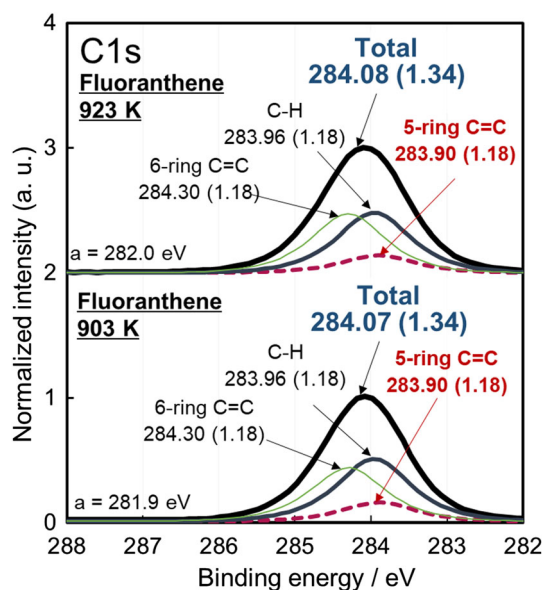
Figure 18 Experimental C1s XPS spectra of fluoranthene heated at 903 and 923 K. As-received fluoranthene could not be analyzed because of the low melting point (383 K). "a" in this figure represents the C1s peak position before correction of peak tops using standard C=C.

decomposed and fluoranthene-like structure, which shows peaks at higher binding energy (283.9 eV), forms as suggested by ReaxFF. In addition, this method to estimate the percentage of pentagons is limited to carbon materials without containing sp^3C and hetero atoms such as oxygen and nitrogen as explained above.

In a similar way to other raw materials, upon the carbonization reaction, coronene molecules were dehydrogenated (Coro2) to form new hexagons (Coro3, 4, and 6). The presence of Coro2–4, and 6 was estimated by comparing experimental and calculated peak positions in IR and Raman spectra (Figs. 10 and 14) in addition to ReaxFF (Fig. 6c). Structures similar to Coro2 were obtained from the results of ReaxFF in Fig. 6c-1. Structures similar to Coro3 were also obtained by heating the structure Cora2 using ReaxFF (Fig. 6c-2). Calculated C1s XPS spectrum of Coro1 includes only two peaks such as C=C in hexagons and C–H at 284.30 eV and 284.03 eV, respectively (Table 8 and Fig. 19). Carbonized coronene showed much smaller experimental FWHM, 1.32 eV (Fig. 20), than carbonized corannulene (1.46–1.51 eV) (Fig. 16) and carbonized fluoranthene (1.34 eV) (Fig. 18). Thus, the percentage of pentagons was estimated to be 0% (Table 9).

SEM

Figures 21 and S7a show scanning electron microscope (SEM) images of the surface morphology of carbonized corannulene, fluoranthene, and coronene. Corannulene carbonized at 858–923 K resulted in films with grained texture on the surface, whereas corannulene carbonized at 943 and 973 K showed a smooth surface with cracks. The presence of cracks in the film is caused by the shrinkage of films during carbonization on quartz plates. The generation of cracks can be suppressed by preparing thinner films, use of substrates with rough surface for mechanical rocking between carbon films and the substrates, or adding fillers such as carbon nanotubes [76, 77]. Spherical particles with 1–40, 5–30, and 0.5–1 μm in diameter were found on the surface at 858, 873, and 923 K, respectively, probably because the presence of pentagons formed spherical particles in addition to the formation of films. Spheres on the films were also observed in the cross section of corannulene carbonized at 873 K (Figure S7b). The absence of spherical particles in the corannulene films carbonized at 943 and 973 K implies either the absence

Table 7 Areal percentages of C=C and C–H in experimental C1s XPS spectra of fluoranthene and fluoranthene heated at 903 and 923 K

Structure	Areal percentage of carbon/%				Ratio from elemental analyses[a]
	Pentagonal C=C (%)	Hexagonal C=C	Standard C=C	C–H	C=C:C–H
Fluoranthene (calculated)[b]	31 (100)	0	6	63	6:10
Fluoranthene 903 K	14 (45)	40	0	46	8.7:7.3
Fluoranthene 923 K	13 (42)	43	0	44	8.9:7.1

(): Percentages in parenthesis indicate the remained percentages of pentagon in carbonized samples

[a]Results of elemental analysis was obtained from Table 1

[b]As-received fluoranthene could not be analyzed because of the low melting point. Thus, the calculated percentage is shown

Table 8 Calculated peak positions of C1s XPS spectra for coronene (Coro1), dehydrogenated coronene (Coro 2), and further dehydrogenated coronene (Coro3)

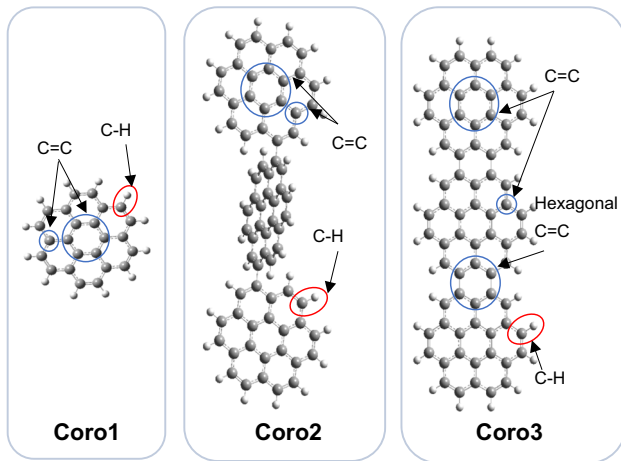| Structure	Calculated C1s peak position/eV			
	Pentagonal C=C	Hexagonal C=C	Standard C=C	C–H
Coro1	0.00	0.00	284.30	284.03
Coro2	0.00	0.00	284.37	284.03
Coro3	0.00	284.44	284.23	283.96

Figure 19 Structures of coronene (Coro1), dehydrogenated coronene (Coro2), and the further dehydrogenated coronene (Coro3) used for assignments of C1s XPS spectra.
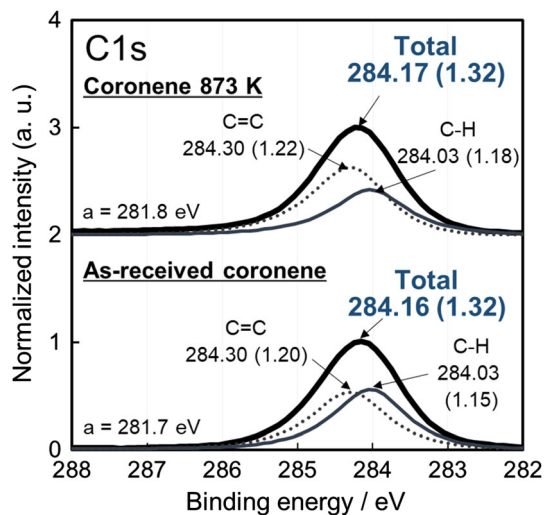

Figure 20 Experimental C1s XPS spectra of as-received coronene and coronene heated at 873 K. "a" in this figure represents the C1s peak position before correction of peak tops using standard C=C.

of pentagons or the low percentage of pentagons at the temperatures. Because of the ability to form films on substrates, it is possible to coat the surface of various supports as explained in our previous works such as silica, carbon nanotube, and more supports with high surface area [78, 79].

Electrical resistivity and band gap

Table 10 shows the electrical resistivity of carbonized corannulene, fluoranthene, and coronene. Corannulene forms film at 823 K, whereas fluoranthene and coronene formed films at 903 and 923 K (Table 1), respectively. These films showed electrical resistivities in the range of semiconductor. Corannulene heated at 858 K or lower was not measurable because of the high electrical resistivities, but measurable at 873 K (1.1×10^4 Ω meter). Corannulene heated at 923 K (1.5×10^3 Ω meter) showed lower electrical resistivity than that heated at 973 K (5.7×10^3 Ω meter) probably because of the absence of cracks on the film (Fig. 21). Electrical resistivity of corannulene carbonized at 923 K (1.5×10^3 Ω meter) was much higher than reported electrical resistivity of carbonized epoxy resin (3.5×10^{-2} Ω meter) and a little higher than that of pitch film carbonized at 923 K (5×10^2 Ω meter) [77]. One of the plausible reasons for the high electrical resistivity is that the presence of pentagons and the curvature increased the band gaps of carbonized materials as explained by Menon et al. [61]. As shown in the calculated results in Figure S8, the bandgap of Cora1 was the highest among Cora1 (4.38 eV), Fluo1 (4.02 eV), and Coro1 (4.04 eV). The band gaps of the corannulene dimer (3.05 eV) and trimers (2.82 and 2.87 eV) were basically still larger than those of fluoranthene and coronene dimer, trimer, and hexamer.

Table 9 Areal percentages of C=C and C–H in experimental C1s XPS spectra of as-received coronene and coronene heated at 873 K

Structure	Experimental areal percentage of carbon/%				Ratio from elemental analyses[a]
	Pentagonal C=C	Hexagonal C=C	Standard C=C	C–H	C=C:C–H
As-received coronene	0	0	50	50	12:12
Coronene 873 K[b]	0	0	59	41	–

[a]The result of elemental analysis was obtained from Table 1

[b]The areal percentage of coronene heated at 873 K was estimated using peak position of as-received coronene

Figure 21 SEM images of carbonized corannulene (**a**), fluoranthene (**b**), and coronene (**c**). **a1** Corannulene carbonized at 858 K. **a2** 873 K. **a3** 903 K. **a4** 923 K. **a5** 943 K. **a6** 973 K. **b** Fluoranthene carbonized at 943 K. **c** Coronene carbonized at 1023 K. The size of scale bar is 100 micro meters.
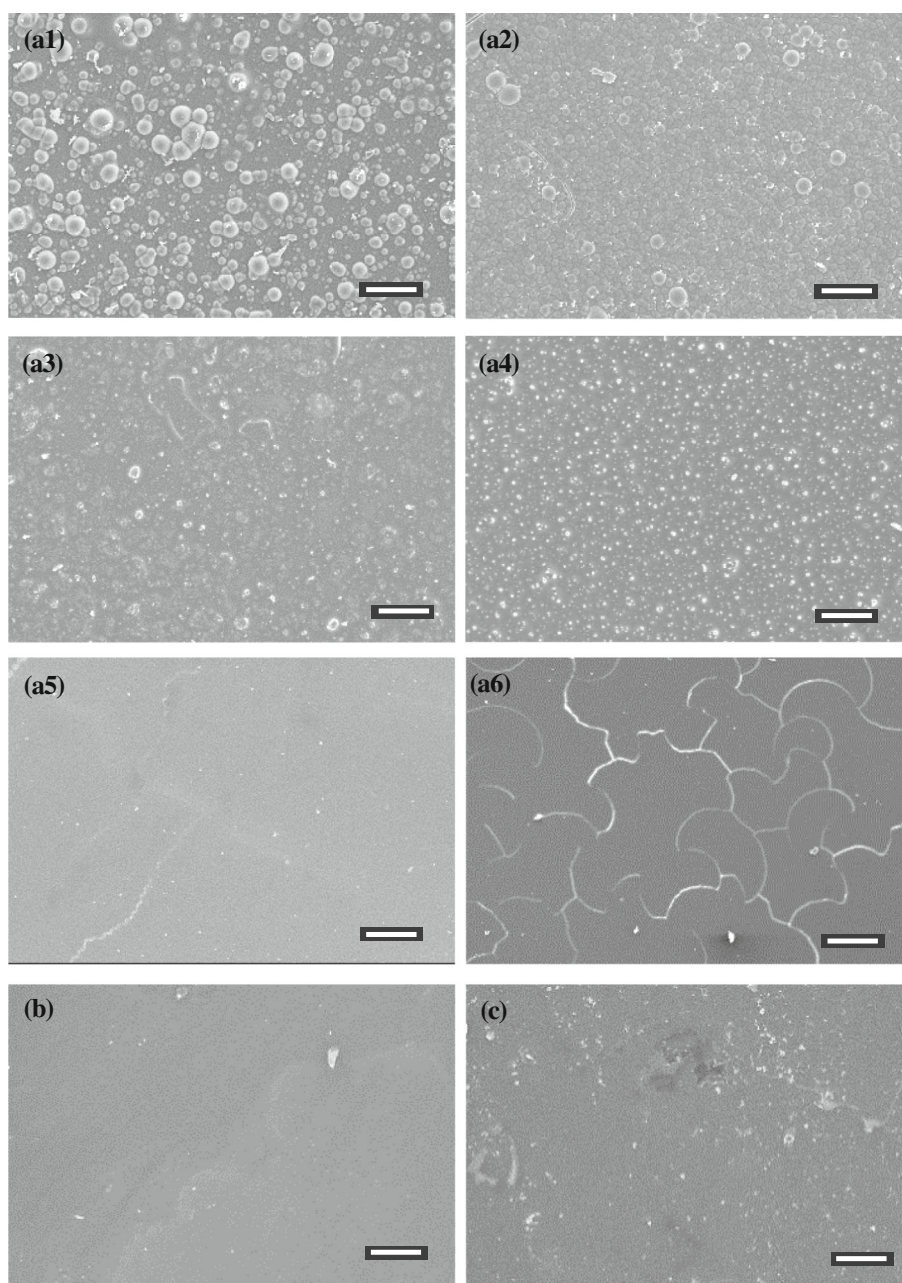
Table 10 Electrical resistivity of carbonized film of corannulene, fluoranthene, and coronene on quartz plates compared to the reported electrical resistivity of carbon films prepared from other raw materials

Sample name (carbonized temperature)	Electrical resistivity/Ohm meter
Corannulene (858 K)	N. A.*
Corannulene (873 K)	1.1×10^4
Corannulene (903 K)	1.6×10^3
Corannulene (923 K)	1.5×10^3
Corannulene (943 K)	2.6×10^3
Corannulene (973 K)	5.7×10^3
Fluoranthene (943 K)	1.4×10^3
Fluoranthene (973 K)	1.6×10^2
Coronene (1023 K)	2.3×10^1
Epoxy resin (923 K)*	3.5×10^{-2}
Pitch (923 K)*	5×10^2

*Values were obtained from a reference [74]

Conclusions

Carbon films with high pentagon density could be prepared by carbonizing corannulene at 823–923 K and fluoranthene at 903 K, whereas carbon films with predominantly hexagons could be prepared by carbonizing coronene at 923 K. Fullerene with pentagons remained as black powder even after heat treatment up to 1173 K. The high reactivity of corannulene compared to those of fluoranthene, coronene, and fullerene relates to the presence of hydrogen and pentagons in corannulene as suggested by ReaxFF simulation in addition to the bond length at DUO positions and the loss of aromaticity in corannulene. The presence of different types of pentagons in carbonized corannulene and fluoranthene was revealed by the presence of peaks in experimental and simulated IR and Raman spectra. Furthermore, broad peaks observed in C1s XPS spectra of carbonized corannulene and fluoranthene also indicate the presence of pentagons as results of simulated C1s XPS spectra of dehydrogenated raw materials. The estimation of the percentage of pentagons in carbon materials using experimental C1s XPS and elemental analysis with the aid of calculated C1s XPS spectra has been conducted experimentally for the first time. The percentages of remained pentagons in corannulene carbonized at 823 K and fluoranthene carbonized at 903 K were estimated to be 52 and 45% by assuming the percentage of pentagons in corannulene and fluoranthene to be 100%, respectively. However, as the heat-treatment temperatures increased, the percentage of pentagons in corannulene and fluoranthene decreased. The decrement of pentagons is initiated primarily by the scission of C=C in hexagons, leading to the scission of C=C in pentagons as results of molecular dynamics simulation with a reactive force field. In addition, carbon films prepared from corannulene at 873 K contained 7% of pentagons (40% of pentagons compared to the raw material) and had measurable electrical resistivity (1.1×10^4 Ω meter), demonstrating that the carbon materials can be applied to electrodes.

Acknowledgement

References

[1] Kroto HW, Heath JR, O'Brien SC, Curl RF, Smalley RE (1985) C$_{60}$: Buckminsterfullerene. Nature 318:162–163

[2] Iijima S (1991) Helical microtubules of graphitic carbon. Nature 354:56–58

[3] Novoselov KS, Geim AK, Morozov SV, Jiang D, Zhang Y, Dubonos SV et al (2004) Electric field effect in atomically thin carbon films. Science 306:666–669

[4] Novoselov KS, Geim AK, Morozov SV, Jiang D, Katsnelson MI, Grigorieva IV et al (2005) Two-dimensional gas of massless Dirac fermions in graphene. Nature 438:197–200

[5] Zhu J, Huang Y, Mei W, Zhao C, Zhang C, Zhang J et al (2019) Effects of intrinsic pentagon defects on

electrochemical reactivity of carbon nanomaterials. Angew Chem Int 58:1–7

[6] Narita K, Okada S (2016) Geometric and electronic structures of corannulene polymers: ultra narrow graphene ribbons with corrugation and topological defects. Chem Phys Lett 650:76–81

[7] Wei Y, Wu J, Yin H, Shi X, Yang R, Dresselhaus M (2012) The nature of strength enhancement and weakening by pentagon-heptagon defects in graphene. Nat Mater 11:759–763

[8] Cai J, Ruffieux P, Jaafar R, Bieri M, Braun T, Blankenburg S et al (2010) Atomically precise bottom-up fabrication of graphene nanoribbons. Nature 466:470–473

[9] Ruffieux P, Wang S, Yang B, Sánchez-Sánchez C, Liu J, Dienel T, Talirz L, Shinde P et al (2016) On-surface synthesis of graphene nanoribbons with zigzag edge topology. Nature 531:489–493

[10] Yamada Y, Gohda S, Abe K, Togo T, Shimano N, Sasaki T et al (2017) Carbon materials with controlled edge structures. Carbon 122:694–701

[11] Yamada Y, Kawai M, Yorimitsu H, Otsuka S, Takanashi M, Sato S (2018) Carbon materials with zigzag and armchair edges. ACS Appl Mater Interfaces 10:40710–40739

[12] Georgakilas V, Otyepka M, Bourlinos AB, Chandra V, Kim N, Kemp KC et al (2012) Functionalization of graphene: covalent and non-covalent approaches, derivatives and applications. Chem Rev 112:6156–6214

[13] Bottari G, Herranz MA, Wibmer L, Volland M, Rodrıguez-Perez L, Guldi DM et al (2017) Chemical functionalization and characterization of graphene-based materials. Chem Soc Rev 46:4464–4500

[14] Kim J, Yamada Y, Suzuki Y, Ciston J, Sato S (2014) Pyrolysis of epoxidized fullerenes analyzed by spectroscopies. J Phys Chem C 118:7076–7084

[15] Jiang Y, Yang L, Sun T, Zhao J, Lyu Z, Zhuo O et al (2015) Significant contribution of intrinsic carbon defects to oxygen reduction activity. ACS Catal 5:6707–6712

[16] Han MY, Özyilmaz B, Zhang Y, Kim P (2007) Energy band-gap engineering of graphene nanoribbons. Phys Rev Lett 98:206805

[17] Cui L, Ren X, Wang J, Sun M (2020) Synthesis of homogeneous carbon quantum dots by ultrafast dual-beam pulsed laser ablation for bioimaging. Mater Today Nano 12:10009

[18] Mu X, Sun M (2020) The linear and non-linear optical absorption and asymmetrical electromagnetic interaction in chiral twisted bilayer graphene with hybrid edges. Mater Today Phys 14:100222

[19] Banhart F, Kotakoski J, Krasheninnikov AV (2011) Structural defects in graphene. ACS Nano 5:26–41

[20] Huang PY, Ruiz-Vargas CS, van der Zande AM, Whitney WS, Levendorf MP, Kevek JW et al (2011) Grains and grain boundaries in single-layer graphene atomic patchwork quilts. Nature 469:389–392

[21] Scott LT, Boorum MM, McMahon BJ, Hagen S, Mack J, Blank J, Wegner H, De Meijere A (2002) A rational chemical synthesis of C_{60}. Science 295:1500–1503

[22] Amsharov KY, Jansen MA (2008) C_{78} Fullerene precursor: toward the direct synthesis of higher fullerenes. J Org Chem 73:2931–2934

[23] Ono S, Toda Y, Onoe J (2014) Unified understanding of the electron-phonon coupling strength for nanocarbon allotropes. Phys Rev B 90:155435

[24] Iwasa Y, Arima T, Fleming RM, Siegrist T, Zhou O, Haddon RC et al (1994) New phases of C_{60} synthesized at high pressure. Science 264:1570–1572

[25] Nuñez-Regueiro M, Marques L, Hodeau JL, Béthoux O, Perroux M (1995) Polymerized fullerite structures. Phys Rev Lett 74:278–281

[26] Muzammil EM, Halilovic D, Stuparu MC (2019) Synthesis of corannulene-based nanographenes. Commun Chem 2:58

[27] Nestoros E, Stuparu MC (2018) Corannulene: a molecular bowl of carbon with multifaceted properties and diverse applications. Chem Commun 54:6503–6519

[28] Zabula AV, Filatov AS, Spisak SN, Rogachev AY, Petru-khina MA (2011) A main group metal sandwich: five lithium cations jammed between two corannulene tetraanion decks. Science 333:1008–1011

[29] Yanney M, Fronczek FR, Henry WP, Beard DJ, Sygula A (2011) Cyclotrimerization of corannulyne: steric hindrance tunes the inversion barriers of corannulene bowls. Eur J Org Chem 2011:6636–6639

[30] Kato K, Segawa Y, Scott LT, Itami K (2018) A quintuple [6]helicene with a corannulene core as a C5-symmetric propeller-shaped p-system. Angew Chem Int Ed 57:1337–1341

[31] Inada Y (2015) Laser-induced carbonization of sumanene derivatives. Osaka University. Dissertation

[32] Fitzer E, Mueller K (1968) Paper No. 167. In: 8th Conference on carbon, Buffalo, 1967. Carbon, vol 6, p 234

[33] Ruland W (1965) X-ray studies on the carbonization and graphitization of acenaphthylene and bifluorenyl. Carbon 2:365–378

[34] Singer LS, Lewis IC (1965) An electron spin resonance study of the carbonization of the aromatic hydrocarbon acenaphthylene. Carbon 2:115–120

[35] Granda M, Santamaria R, Menendez R (2003) Chapter 4 Coal-tar pitch: composition and pyrolysis behavior. In: Radovic LR (ed) Chemistry and Physics of Carbon. Marcel Dekker, Inc, New York, pp 263–330

[36] Mochida I, Miyasaka H, Fujitsu H, Takeshita K (1978) Carbonization properties of aromatic hydrocarbons containing five-membered ring. Tanso 92:7–16 **(written in Japanese)**

[37] Khlobystov AN (2011) Carbon nanotubes: from nano test tube to nano-reactor. ACS Nano 5:9306–9312

[38] Zurek E, Pickard CJ, Autschbach J (2008) Density functional study of the ^{13}C NMR chemical shifts in single-walled carbon nanotubes with Stone-Wales defects. J Phys Chem C 112:11744–11750

[39] Sun G, Kertesz M (2000) Theoretical ^{13}C NMR spectra of IPR isomers of fullerenes C_{60}, C_{70}, C_{72}, C_{74}, C_{76}, and C_{78} studied by density functional theory. J Phys Chem A 104:7398–7403

[40] Hawelek L, Wrzalik W, Brodka A, Dore JC, Hannon AC, Iijima S et al (2011) A pulsed neutron diffraction study of the topological defects presence in carbon nanohorns. Chem Phys Lett 502:87–91

[41] Kim J, Yamada Y, Kawai M, Tanabe T, Sato S (2015) Spectral change of simulated X-ray photoelectron spectroscopy from graphene to fullerene. J Mater Sci 50:6739–6747. https://doi.org/10.1007/s10853-015-9229-0

[42] Yamada Y, Yasuda H, Murota K, Nakamura M, Sodesawa T, Sato S (2013) Analysis of heat-treated graphite oxide by X-ray photoelectron spectroscopy. J Mater Sci 48:8171–8198. https://doi.org/10.1007/s10853-013-7630-0

[43] Yamada Y, Sato S (2015) Structural analysis of carbon materials by X-ray photoelectron spectroscopy using computational chemistry. Tanso 269:181–189 **(written in Japanese)**

[44] Yamada Y, Kim J, Matsuo S, Sato S (2014) Nitrogen-containing graphene analyzed by X-ray photoelectron spectroscopy. Carbon 70:59–74

[45] Yamada Y, Matsuo S, Abe K, Kubo S, Sato S (2016) Selective doping of nitrogen into carbon materials without catalysts. J Mater Sci 51:8900–8915. https://doi.org/10.1007/s10853-016-0142-y

[46] Fujimoto A, Yamada Y, Koinuma M, Sato S (2016) Origins of sp^{3}C peaks in C1s X-ray photoelectron spectra of carbon materials. Anal Chem 88:6110–6114

[47] Kim J, Lee N, Nodo M, Min YH, Noh SH, Kim N et al (2018) Distinguishing zigzag and armchair edges on graphene nanoribbons by X-ray photoelectron and Raman spectroscopies. ACS Omega 3:17789–17796

[48] Nishihara H, Hirota T, Matsuura K, Ohwada M, Hoshino N, Akutagawa T et al (2017) Synthesis of ordered carbonaceous frameworks from organic crystals. Nat Commun 8:109

[49] Saha B, Schatz GC (2012) Carbonization in polyacrylonitrile (PAN) based carbon fibers studied by ReaxFF molecular dynamics simulations. J Phys Chem B 116:4684–4692

[50] Li K, Zhang H, Li G, Zhang J, Bouhadja M, Liu Z et al (2018) ReaxFF molecular dynamics simulation for the graphitization of amorphous carbon: a parametric study. J Chem Theory Comput 14:2322–2331

[51] Senda T, Yamada Y, Morimoto M, Nono N, Sogabe T, Kubo S et al (2019) Analyses of oxidation process for isotropic pitch-based carbon fiber using model compounds. Carbon 142:311–326

[52] Sasaki T, Yamada Y, Sato S (2018) Quantitative analysis of zigzag and armchair edges on carbon materials with and without pentagons using infrared spectroscopy. Anal Chem 90:10724–10731

[53] Yamada Y, Murota K, Fujita R, Kim J, Watanabe A, Nakamura M et al (2014) Subnanometer vacancy defects introduced on graphene by oxygen gas. J Am Chem Soc 136:2232–2235

[54] Eckmann A, Felten A, Mishchenko A, Britnell L, Krupke R, Novoselov KS et al (2012) Probing the nature of defects in graphene by Raman spectroscopy. Nano Lett 12:3925–3930

[55] Malard LM, Pimenta MA, Dresselhaus G, Dresselhaus MS (2009) Raman spectroscopy in graphene. Phys Rep 473:51–87

[56] Nemanich RJ, Solin SA (1979) First- and second-order Raman scattering from finite-size crystals of graphite. Phys Rev B 20:392–401

[57] IUPAC (1997) Compendium of Chemical Terminology, 2nd ed. (the "Gold Book"). Compiled by McNaught AD and Wilkinson A Blackwell Scientific Publications, Oxford (1997). Online version (2019-) created by Chalk SJ. ISBN 0-9678550-9-8. https://doi.org/10.1351/goldbook.C00840

[58] Frisch MJ, Trucks GW, Schlegel HB, Scuseria GE, Robb MA, Cheeseman JR et al (2009) Gaussian 09, revision E.01. Gaussian Inc, Wallingford, CT

[59] Computational Chemistry Comparison and Benchmark Data Base, NIST, https://cccbdb.nist.gov/vibscalejust.asp, as of July 2, 2020

[60] Liu L, Liu Y, Zybin SV, Sun H, Goddard WA III (2011) ReaxFF-lg: correction of the ReaxFF reactive force field for London dispersion, with applications to the equations of state for energetic Materials. J Phys Chem A 115:11016–11022

[61] Menon A, Dreyer JAH, Martin JW, Akroyd J, Robertson J, Kraft M (2019) Optical band gap of cross-linked, curved, and radical polyaromatic hydrocarbons. Phys Chem Chem Phys 21:16240–16251

[62] Terrones M, Terrones H, Banhart F, Charlier J, Ajayan P (2000) Coalescence of single-walled carbon nanotubes. Science 288:1226–1229

[63] Martin JW, McIntosh GJ, Arul R, Oosterbeek RN, Kraft M, Söhnel T (2017) Giant fullerene formation through thermal treatment of fullerene soot. Carbon 125:132–138

[64] Gutman I, Ruiz-Morales Y (2007) Note on the Y-rule in Clar theory. Polycycl Aromat Comp 27:41–49

[65] Solà M (2013) Forty years of Clar's aromatic π-sextet rule. Front Chem 1:22

[66] Chung DDL (2003) Review graphite. J Mater Sci 37:1475–1489. https://doi.org/10.1023/A:1014915307738

[67] Martin JW, Hou D, Menon A, Pascazio L, Akroyd J, You X, Kraft M (2019) Reactivity of polycyclic aromatic hydrocarbon soot precursors:implications of localized π-radicals on rim-based pentagonal rings. J Phys Chem C 123:26673–26682

[68] Whitesides R, Frenklach M (2010) Detailed kinetic Monte Carlo simulations of graphene-edge growth. J Phys Chem A 114:689–703

[69] Singh RI, Mebel AM, Frenklach M (2015) Oxidation of graphene-edge six- and five-member rings by molecular oxygen. J Phys Chem A 119:7528–7547

[70] Violi A (2005) Cyclodehydrogenation reactions to cyclopentafused polycyclic aromatic hydrocarbons. J Phys Chem A 109:7781–7787

[71] Chanyshev AD, Litasov KD, Shatskiy AF, Furukawa Y, Yoshino T, Ohtani E (2015) Oligomerization and carbonization of polycyclic aromatic hydrocarbons at high pressure and temperature. Carbon 84:225–235

[72] Ōsawa S, Ōsawa E, Hirose Y (1995) Doubly bonded C_{60} dimers and congeners: computational studies of structures, bond energies and transformations. Fullerene Sci Technol 3:565–585

[73] Sabirov DS (2013) Polarizability of C_{60} fullerene dimer and oligomers: the unexpected enhancement and its use for rational design of fullerene-based nanostructures with adjustable properties. RSC Adv 3:19430–19439

[74] Koshino M, Niimi Y, Nakamura E, Kataura H, Okazaki T, Suenaga K, Iijima S (2010) Analysis of the reactivity and selectivity of fullerene dimerization reactions at the atomic level. Nat Chem 2:117–124

[75] Schettino V, Pagliai M, Ciabini L, Cardini G (2001) The vibrational spectrum of fullerene C_{60}. J Phys Chem A 105:11192–11196

[76] Yamada Y (2008) Chung DDL (2008) Three-dimensional microstructuring of carbon by thermoplastic spacer evaporation during pyrolysis. Carbon 46:1765–1772

[77] Yamada Y, Chung DDL (2008) Epoxy-based carbon films with high electrical conductivity attached to an alumina substrate. Carbon 46:1798–1801

[78] Tanabe T, Yamada Y, Kim J, Koinuma M, Kubo S, Shimano N, Sato S (2016) Knoevenagel condensation using nitrogen-doped carbon catalysts. Carbon 109:208–220

[79] Khan SM, Kitayama H, Yamada Y, Gohda S, Ono H, Umeda D, Abe K, Hata K, Ohba T (2018) High CO_2 sensitivity and reversibility on nitrogen-containing polymer by remarkable CO_2 adsorption on nitrogen sites. J Phys Chem C 122:24143–24149